Design of molecularly imprinted polymer materials relying on hydrophobic interactions

Najeh Jaoued-Grayaa, Chaima Nasraoui, Yves Chevalier, Souhaira Hbaieb

DESIGN OF MOLECULARLY IMPRINTED POLYMER MATERIALS RELYING ON HYDROPHOBIC INTERACTIONS

Najeh Jaoued-Grayaa[1], Chaima Nasraoui[2,3], Yves Chevalier[3,*] and Souhaira Hbaieb[2,*]

1- *Unité Spécialisée de développement des techniques analytiques, Institut National de Recherche et d'Analyse Physico-chimique, Biotechpole Sidi-Thabet, 2020 Ariana, Tunisia.*

2- *Laboratoire de Recherche: Caractérisations, Applications et Modélisation de Matériaux, Université de Tunis El Manar, Faculté des Sciences de Tunis, Campus universitaire El Manar, Tunisia.*

3- *Laboratoire d'Automatique, de Génie des Procédés et de Génie Pharmaceutique, Université de Lyon 1, UMR 5007 CNRS, 43 bd 11 Novembre, 69622 Villeurbanne, France.*

* Corresponding authors:

Souhaira Hbaieb: souhaira.hbaieb@fst.utm.tn

Tel: +216 71 88 34 24; Fax: +216 71 80 25 36

Yves Chevalier: yves.chevalier@univ-lyon1.fr

Tel: +33 472 43 18 77

Abstract

The design of molecularly imprinted polymers (MIPs) for the specific binding of hydrophobic molecules (mitotane) was investigated by considering monomers and cross-linking agents with variable hydrophobic character, methyl methacrylate, butyl methacrylate and lauryl methacrylate as functional monomers, and ethylene glycol dimethacrylate and 1,6-hexanediol dimethacrylate as cross-linking agents. MIPs were bound to a porous silica support by means of a radical transfer reaction with grafted 3-mercaptopropyl groups. Equilibrium adsorption isotherms to molecularly imprinted and non-imprinted materials were modeled with the Volmer and Langmuir–Volmer isotherms, giving the thermodynamic parameters of adsorption. The most hydrophobic monomer provided the highest selective adsorption although strong non-selective adsorption and the intrinsic softness of poly(lauryl methacrylate) is detrimental to selectivity. Adsorption was exothermic with a predominant enthalpic contribution. Adsorption kinetics were fast due to the high accessibility of molecular imprints on the surface of the thin MIP layer coating the porous silica support.

Keywords: Molecularly imprinted polymer; Hydrophobic interactions; Selective adsorption; Adsorption isotherm; Mitotane.

1. Introduction

Molecular imprinting a polymer material is widely used to obtain a synthetic solid material named “Molecular Imprinted Polymer” (MIP) able to bind a specific molecule compared to its non-imprinted counterpart (NIP) [1,2]. The imprinting process involves the copolymerization of a functional monomer with a large amount of a cross-linking agent in the presence of the molecule acting as a template. Removal of the template from the rigid cross-linked polymer material leaves “specific cavities” (molecular imprints) keeping the shape-memory of the target molecule. This methodology requires that rather strong interactions of the target molecule with the monomer occur during the synthesis and with the polymer in the molecular imprints for specific binding. Strong interactions with the monomer are often taken as clues for selective interactions with the polymer material. They are most often investigated by theoretical chemistry tools [3,4]. Specific molecular recognition relies on directional interactions, mostly hydrogen bonds. MIPs based on the acrylic acid functional monomer are widely studied because the weak carboxylic acid groups may bind by hydrogen bonds to many weakly basic compounds [1,4–7]. Many types of other functional monomers having hydrogen bonding ability have been considered [3,6–10]. Isotropic interactions such as electrostatic ones may be strong but their isotropic nature make them unspecific. Hydrophobic interactions between molecules have an intermediate directional behavior. In case of lack of strong directed interactions, the design of MIPs is a difficult task as only the formation of a shape-specific cavity may provide specific binding. A favorable shape complementarity allows a better contact of molecules; but the several possible configurations of flexible molecules compromise the selectivity. Non-selective hydrophobic interactions may be combined with selective directional interactions (i.e. hydrogen bonds). Supplementation of selective interactions by non-selective hydrophobic interactions may enhance the overall selectivity. A clue supporting this idea is the work by Wong et al. [11] showing that hydrophobic MIPs based on methacrylic acid allow selective adsorption of diuron

whereas MIPs based on acrylic acid is not selective (MIP = NIP). Therefore, it is presently hypothesized that molecules may selectively bind to hydrophobic molecular imprints provided the latter are rigid enough or they combine hydrophobic and specific directional interactions. The design of MIPs for the specific adsorption of hydrophobic molecules is the topic of the present work. The objective is to address this question by investigating the adsorption behavior of a hydrophobic molecule to MIPs of variable hydrophobic character.

In the present work, MIPs based on polyacrylate polymers were prepared in order to get better understanding about their behavior relying on hydrophobic interactions. Poly(alkylmethacrylate) materials with different alkyl chain lengths (methyl, butyl and dodecyl) cross-linked with either ethylene glycol dimethacrylate (EGDMA) or hexanediol dimethacrylate (HDDMA) have been investigated so as to disclose structure-activity relationships and select an optimized material. Adsorption isotherms, adsorption kinetics and thermodynamic studies were carried out to get insight on the fundamentals of the adsorption process of a hydrophobic model molecule onto the series of adsorbents.

Mitotane (Mit), 1-(2-chlorophenyl)-l-(4-chlorophenyl)-2,2-dichloroethane (o,p'-DDD), was taken as the model hydrophobic molecule; its water-octanol partition coefficient is given by log$P$ = log($K_{o\text{-}w}$) = 5.87. Mit is present at 10 % level in the technical grade insecticide dichlorodiphenyldichloroethane (DDD) [12] and it is a degradation product of DDT. Although these chemicals have been banned for their use as pesticides and the treatment of head lice, they are still present in animal tissues and in the environment, especially ground waters, because of their long persistence [13]. Their detection and quantification in water are therefore mandatory actions. Moreover, mitotane is used as a chemotherapy drug to treat a rare cancer of the adrenal glands (adrenal cortical carcinoma) [14,15]. This toxic agent must be administrated at doses lower than 20 mg·L^{-1} to minimize its side effects and its concentration needs must be monitored in the patient's blood [16]. Ground water and blood are two complex matrices, which make the

detection of mitotane impossible by means of a direct HPLC analysis. A pre-concentration step by SPE prior to analysis is required. Mitotane is a hydrophobic molecule, poorly soluble in water that needs being extracted from aquatic matrices. MIPs have been widely employed as adsorbents in SPE technique to extract organic contaminants from water samples. However, mitotane as an organochlorine compound similar to many organochlorine pesticides in structure does not have available polar functional groups suitable to interact with monomer using non-covalent interactions like hydrogen bonding. For such poorly functional molecules taken from aqueous media, the development of MIPs relies on hydrophobic and π-π interactions as it has been shown in the case of benzopyrene [17].

Analysis of molecules present as dilute solutions in complex media such as environmental samples requires a pre-concentration step by selective extraction. Solid phase extraction (SPE) is mostly used for the extraction of analytes as an alternative technique for liquid-liquid extraction (LLE) protocols [18]. The extraction technique on solid supports is a fast and efficient method that offers high extraction yield and consumes less organic solvent. It allows extraction from complex matrices and further analysis with quantification limits of ten or hundred $ng \cdot L^{-1}$ [19]. As an example, an efficient method has been developed to concentrate Mit on a Discovery DSC18 cartridge from various biological fluids such as red blood cells, plasma, and urine samples from patients chronically treated with 1.5 g of MIT and analyze it by HPLC [20]. However, the extraction and purification of the active molecules remain a delicate step due to the possible presence of numerous interfering compounds. Instead of using SPE cartridges based on C18-modified silica or polystyrene solid materials with low selectivity [21], it is interesting to prepare a selective adsorbent based on a shape-selective molecular recognition mechanism [22–24].

2. Materials and Methods

2.1. Materials

Fumed silica Cab-O-Sil with a mean size of primary particles of 7 nm and a specific area of 200 $m^2 \cdot g^{-1}$ was obtained from Cabot Corporation (Tuscold, ILL) and was dried at 140 °C for 3 h under vacuum before use. Mitotane (Sigma–Aldrich) with 99 % purity was used as the template. 3-Mercaptopropyltrimethoxysilane (3-MPTMS, Sigma–Aldrich) was used as a silane coupling agent. Methyl methacrylate (MMA), butyl methacrylate (BMA) and lauryl methacrylate (LMA) were employed as functional monomers (Sigma–Aldrich, 99 %). Azobis-isobutyronitrile (AIBN, Sigma–Aldrich) was used as the initiator of polymerization. Ethylene glycol dimethacrylate (EGDMA, Sigma–Aldrich, 98 %) and 1,6-hexanedioldimethacrylate (HDDMA, Sigma–Aldrich, 98 %) were employed as a cross-linking agents. Toluene was dried and distilled before use. N-ethyldiisopropylamine was purchased from Sigma–Aldrich and used as received. All solvents, acetonitrile, methanol and tetrahydrofuran (THF), were purchased from Fisher Scientific as HPLC grade. Water was double-deionized and filtered with a 0.45 μm filter membrane before use.

2.2. Methods

IR spectra were recorded with a Bruker IFS 55 Equinox FTIR spectrometer. The Raman spectrum was recorded using Jobin–Yvon spectrometer (T64000 model) equipped with an Ar^+ laser providing an excitation wavelength of 488 nm and a CCD detector in a back-scattering geometry. ^{29}Si and ^{13}C NMR spectra of silica materials were carried out on a Bruker Avance III 500 ultra-shield PLUS spectrometer. The ultraviolet-visible (UV–Vis) spectrophotometer (Varian Cary 50 type) was employed for the measurement of mitotane absorbance. The silica materials were subjected to thermogravimetric analyses (TGA) performed on a DuPont TA Q50 (USA) instrument fitted with a data station. The analysis was carried out from 40 °C to 800 °C at a heating rate of 10 $°C \cdot min^{-1}$ under an air atmosphere. A Perkin–Elmer type and a series II

model CHS analyzer 2400 were used for elemental analyses of carbon, sulfur and hydrogen. Transmission electron microscopy (TEM) observations were performed at the "Centre Technologique des Microstructures" (CTμ) facility of the University of Lyon 1 (http://microscopies.univ-lyon1.fr/) using a Philips CM120 microscope operating at 80 kV acceleration voltage. A drop of 0.1 % aqueous dispersion was deposited on a formvar grid and dried in the open air before TEM observation.

2.3. Synthesis of the imprinted materials

2.3.1. Grafting of 3-MPTMS on the silica surface

5 g of dried silica was dispersed in anhydrous toluene. After that, 0.5 g of N-ethyldiisopropylamine was added dropwise. Then, 5 g of 3-mercaptopropylmethoxysilane was added to the reaction mixture under a nitrogen atmosphere. The reaction mixture was stirred for 24 h at 80 °C. The SiO_2@MPTMS powder was filtered and washed thoroughly with THF and then dried at 60 °C and stored under vacuum for subsequent uses.

2.3.2. Synthesis of the imprinted and non-imprinted polymers

100 mg of the modified silica SiO_2@MPTMS was dispersed in 4 mL anhydrous acetonitrile with 25.6 mg (0.08 mmol = 4 μmol·m^{-2}) of mitotane dissolved in 1 mL of methanol. The mixture solution was flushed with nitrogen gas for 10 min to remove oxygen and heated at 80 °C. The monomer, cross-linking agent and AIBN (0.3 mg) were added in this order and the polymerization was run for 3 h. The masses of the reagents are indicated in the Table S1. At the end of polymerization, the polymer materials were separated by centrifugation (4000 rpm) for 10 min, rinsed with acetonitrile and dried at 40 °C overnight. Mitotane was removed by washing the materials with methanol in a Soxhlet extractor for 48 h and then dried under reduced pressure. The efficiency of template extraction was checked by the disappearance of

mitotane absorption bands in the UV–Vis analysis of the extraction solvent. As a control, non-imprinted polymer materials were also prepared using the same method without mitotane. The names of prepared MIPs and NIPs are given in Table S1.

2.4. Adsorption of mitotane onto MIPs and NIPs

2.4.1. Calibration curve of UV–Vis absorbance

The standard solutions of concentrations ranging between 75 and 30 µmol·L^{-1} were prepared by appropriate dilution of 5 10^{-4} mol·L^{-1} mitotane solution. Their absorbance at 229 nm wavelength was linear with respect to the concentration.

2.4.2. Adsorption experiments

The material was immersed in 10 mL of methanol/water (50/50, v/v) mixture containing mitotane with various concentrations from 30 to 75 µmol·L^{-1} and kept under magnetic stirring (280 rpm) at 25 °C. The UV–Vis absorbance was measured at the wavelength of maximum absorbance (λ_{max} = 229 nm) for determination of the residual concentration (C, mol·L^{-1}). The adsorption uptake (Q, mol·m^{-2}) and adsorption percentage (%A, %) of mitotane were calculated according to the following Eqs 1 and 2.

$$Q = \frac{V}{m\,A_{SP}}(C_0 - C) \quad (1)$$

$$\%A = (C_0 - C)\frac{100}{C_0} \quad (2)$$

where C_0 is the initial concentration of mitotane, C is the concentration of mitotane collected in the supernatant from a sample in contact with MIP or NIP materials, V is the volume of the mitotane solution, m is the mass of MIP or NIP materials, and A_{SP} is the specific area of the silica support (200 m^2·g^{-1}).

2.4.3. Competitive adsorption experiments

Aqueous solutions containing 100 mg·L^{-1} mittotane, *p,p'*-dichlorodiphenyldichloroethene,

chlorpyrifos and endosulfan were prepared in methanol/water (50/50, v/v) mixture. The experiment was performed by mixing 10 mg of the adsorbent with 5 mL of the prepared mixture. After stirring for 15 min at 400 rpm and at room temperature, the supernatant was separated and analyzed for determination of the residual concentration by UV–Vis at the wavelength of maximum absorbance of each molecule (mitotane: λ_{max} = 229 nm), (*p*,*p*′-dichlorodiphenyldichloroethene: λ_{max} = 230 nm), (chlorpyrifos: λ_{max} = 230 nm) and (endosulfan: λ_{max} = 227 nm).

3. Results and discussion

The surface imprinting technique was chosen to overcome some drawbacks such as accessibility to adsorption sites. Indeed, a thin layer of MIP bound to the surface of a porous solid support improves the accessibility to the recognition sites and accelerates adsorption kinetics [6,25–29], As an example, a thin MIP coating bound to silica powder has been implemented in standard SPE cartridges for the selective pre-concentration of the patulin toxin from apple juices matrices in usual conditions of analysis [28]. As another example, a thin layer of imprinted PANI was immobilized to the porous silica surface by copolymerization of grafted and free aniline for the selective adsorption of the benzophenone-4 sunscreen [27,29].

The thin films of MIP bound to porous silica surface were prepared by modifying the surface a silica solid support designed for chromatography with an organosilane containing a thiol group acting as a radical transfer agent (SiO_2@MPTMS) as outlined in Scheme 1. The radical polymerization of acrylic monomers yielded a thin polyacrylate layer strongly attached to a silica support.

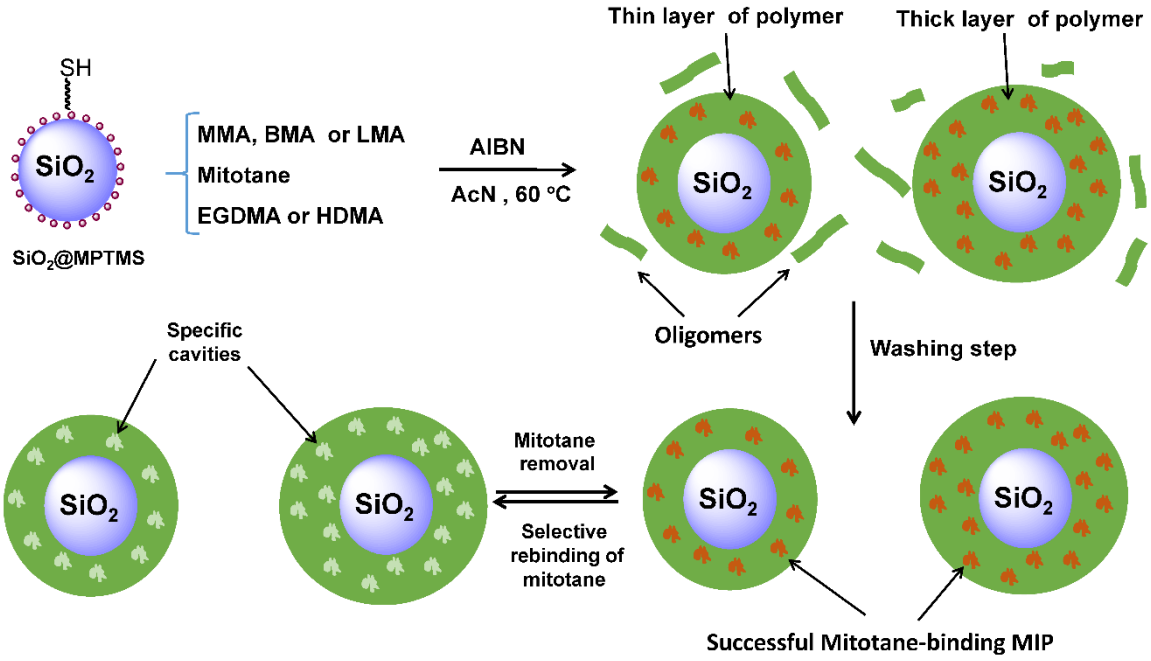

Scheme 1. Schematic illustration of the two steps for the preparation of molecularly imprinted polymer. Step I: Grafting of radical transfer agent (thiol) to silica surface by means of silane coupling agent. Step II: Copolymerization of acrylic monomer and cross-linking agent in the presence of grafted radical transfer agent.

3.1. Preparation of molecularly imprinted polymer nanoparticles

3.1.1. Grafting methacryloyl groups onto silica

3-MPTMS was grafted onto the silica surface to afford initiating groups for subsequent polymerization taking place from the silica surface. 3-MPTMS was covalently attached to the surface of silica nanoparticles by means of a condensation reaction between surface silanol groups of silica and methoxy groups of 3-MPTMS. The resulting SiO_2@MPTMS material was characterized by ^{13}C and ^{29}Si NMR and FTIR spectroscopy, thermogravimetric analysis and elemental analysis reported in details in the Supplementary Information file, and Raman spectroscopy.

The IR spectra of both pristine and grafted silica showed a sharp and strong Si–O–Si stretching band (1010–1190 cm^{-1}), indicating that the main structure of silica has not been changed by the surface modification reaction. The IR spectrum of modified silica shows supplementary bands, at 2928–2858 cm^{-1} corresponding to stretching vibrations of to CH_2 belonging to the organosilane, and a weak band at 2575 cm^{-1} related to stretching vibrations of the S–H group [30]. The latter band was very weak, close to its limit of detection. Clearer evidence of the presence of thiol groups grafted at the surface of silica was given by Raman spectroscopy.

The Raman spectrum of SiO_2@MPTMS (Figure 1) presented the symmetric and asymmetric bands at 2839 and 2945 cm^{-1} corresponding to the methyl and methylene stretching vibrations. Besides, another strong stretching vibration at 2576 cm^{-1} confirmed the existence of –SH functional group of the organosilane 3-MPTMS [31,32]. Raman spectroscopy provided a qualitative confirmation of successful 3-MPTMS grafting onto silica surface. It also showed that the thiol group has been kept intact during the grafting reaction of the organosilane. Oxidation of the thiol groups into disulfide has not been observed.

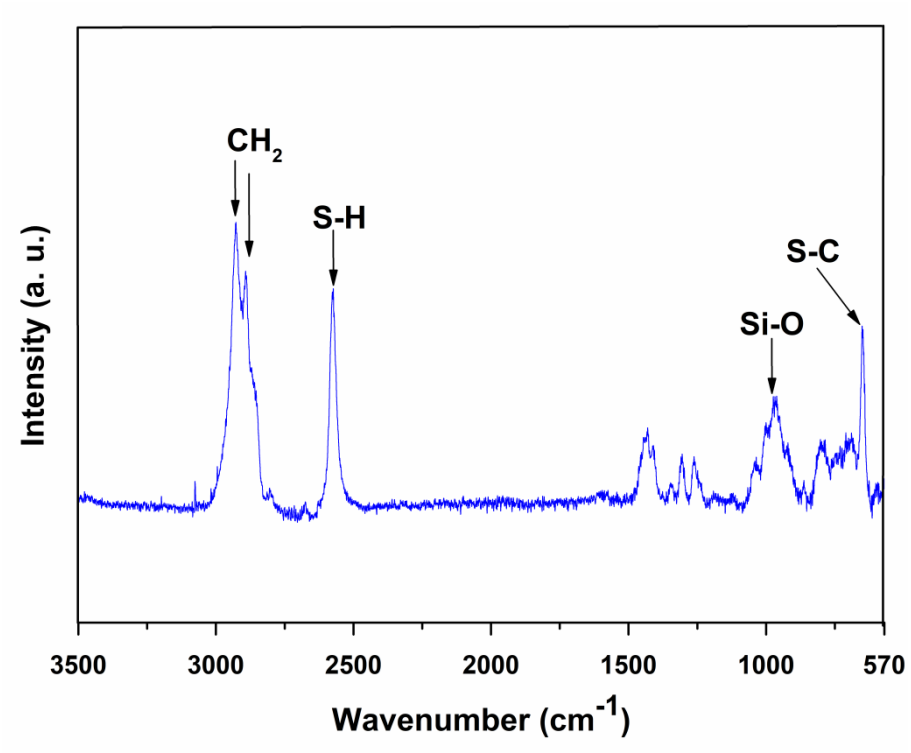

Figure 1. Raman spectrum of SiO_2@MPTMS.

Elemental analysis and thermogravimetric analysis (TGA) were used to determine the coverage of the silica surface by the organosilane. These analyses give the amount of grafted organosilane per unit area silica surface. Elemental analysis gave 3.18 % of sulfur and 4.09 % of carbon in SiO_2@MPTMS, which proved that 3-MPTMS was successfully grafted on silica. The 3-MPTMS grafting density obtained by elemental chemical analysis was calculated from the sulfur content; the interpretation of carbon analysis was uncertain because the condensation of methoxy groups was not complete [6]. The obtained grafting density was 991 $\mu mol \cdot g^{-1}$ (4.95 $\mu mol \cdot m^{-2}$), indicating high efficiency of the one-step grafting process. The grafting density was also calculated from TGA using the mass loss of 7.17 % corresponding to the degradation of grafted 3-MPTMS between 200 and 400 C (Figure S4). The 3-MPTMS grafting density was 962 $\mu mol \cdot g^{-1}$ (4.8 $\mu mol \cdot m^{-2}$). The grafting densities inferred from both methods were in close accordance and in agreement with reports in the literature [33,34].

3.1.2. Synthesis of MIPs

Imprinted polymers as thin film coating the surface of solid support materials avoids burying the template molecules inside the bulk material and provides higher accessibility to the molecular imprints. The silica support was grafted with a mercaptosilane coupling agent, providing anchored initiating –SH groups for subsequent coating the surface of silica with methacrylic polymer during the polymerization step of the process. The thiol groups bound to the surface of SiO_2@MPMTS silica powder allow attaching the polymer to silica by means of a radical transfer reaction. The most common way to attach the polymer to the surface involves copolymerization of the monomer and cross-linker with a monomer (e.g. methacrylate) that has been previously grafted to the surface. Another way is initiating the polymerization from the

surface by the “grafting from” chemistry [35,36]. The present process involving a radical transfer reaction is analogous to the telomerization polymerization process in solution [37]. Three types of monomers of increasing hydrophobic character (LMA, BMA, MMA) and two cross-linkers (EGDMA, HDDMA) were considered. The MIPs were obtained by washing the as-synthesized materials in a Soxhlet extractor with methanol that was selected as an extracting solvent in which the functional monomers and mitotane are both soluble. Such final step of washing created recognition cavities that are complementary in shape and size to template molecules [38]. Non-imprinted polymer (NIP) was produced precisely by the same process, but in absence of mitotane template. In all instances, the characterization of imprinted and non-imprinted materials was made by means of various analysis techniques such as IR spectroscopy, elemental analysis of carbon, TGA and transmission electron microscopy.

The IR spectra of imprinted and non-imprinted materials (Figure 2) revealed similar bands. The bands at 2931 and 2836 cm^{-1} correspond to the methylene groups stretching. Two characteristic bands at 1729 and 1248 cm^{-1} are attributed respectively to the stretching vibration of (C=O) and the elongation vibration of (C–O). The disappearance of the characteristic S–H stretching band of the thiol at 2576 cm^{-1} also gave evidence of radical transfer reactions involving the thiol groups during polymerization. On the other hand, the band corresponding to the C=C group has been considerably weakened. These analyses proved the presence of grafted acrylic polymer on the surface of the modified silica.

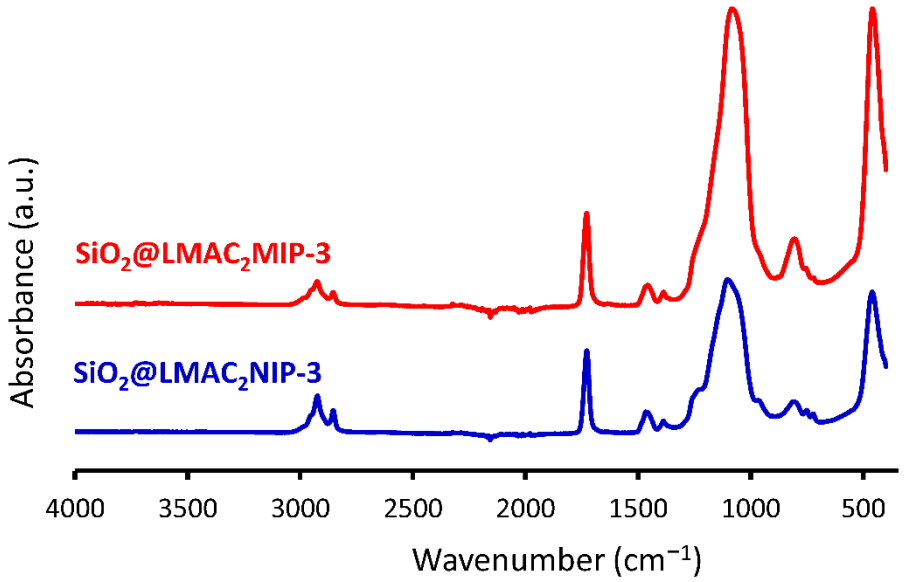

Figure 2. FTIR spectra of SiO_2@LMAC_2MIP-3 and SiO_2@LMAC_2NIP-3.

The elemental analyses giving the carbon content of the materials (Table S2) showed an increase of carbon content (%C ranging between 27 % and 57 %) present in both MIP and NIP with respect to the starting SiO_2@MPTMS (%C = 4.09 %), indicating that polymerization had taken place. Thermogravimetric analyses (TGA) yield the mass losses of materials corresponding to the organic matter grafted onto the surface. TGA traces of SiO_2@LMAC_2MIP-3 and SiO_2@LMAC_2NIP-3 in the temperature range of 200–800 °C are given as example in Figure S4. The mass loss slowly started at 250–350 °C, and was followed by a rapid mass loss above 400 °C resulting from the thermal decomposition of the organic groups of the polymer film coating the silica particles. The dehydroxylation of silanol groups makes a supplementary mass loss that the contribution was eliminated by taking the tangents at temperatures below and above the main mass loss (Figure S5). The TGA data for both imprinted and non-imprinted materials are summarized in Table S2. The TGA mass losses and elemental analyses of carbon are well-correlated. Their ratio is constant: %C/%(mass loss) = 0.67 with a *SD* = 0.02. This means that the organic part of the materials contains 67 % of carbon. It is noted

that the materials prepared from the use of HDDMA as cross-linking agent (C6), gave a higher mass loss compared to those prepared with EGDMA (C2) due to the longer polymethylene chain of HDDMA. The ratio of mass losses of the materials based on HDDMA and EGDMA is constant (mean ratio = 1.07 with *SD* = 0.03), which indicates that both cross-linkers react in a similar way during the polymerization reaction. As expected, the amounts of monomer and cross-linker also affected the mass loss values.

The morphology of the polymer coatings at the surface of SiO_2@MPTMS was assessed by means of TEM pictures. The images of imprinted materials based on copolymerization of LMA and EGDMA at low magnification (Figure 3A) showed a porous material made of strongly aggregated silica nanoparticles. The pictures at high magnification of SiO_2@LMAC_2MIP-3 (Figure 3B) revealed the smooth surface of imprinted nanoparticles which have retained their spherical shape after removal of the mitotane molecules. Moreover, Figure 3B shows some primary particles with grey halo surrounding darker centers, showing the core-shell structure made of silica cores covered with polyacrylate film. The particles are uniform in size, their diameter being in the range 15–30 nm. The small spherical size of primary particles in the imprinted material is beneficial to its adsorption performance.

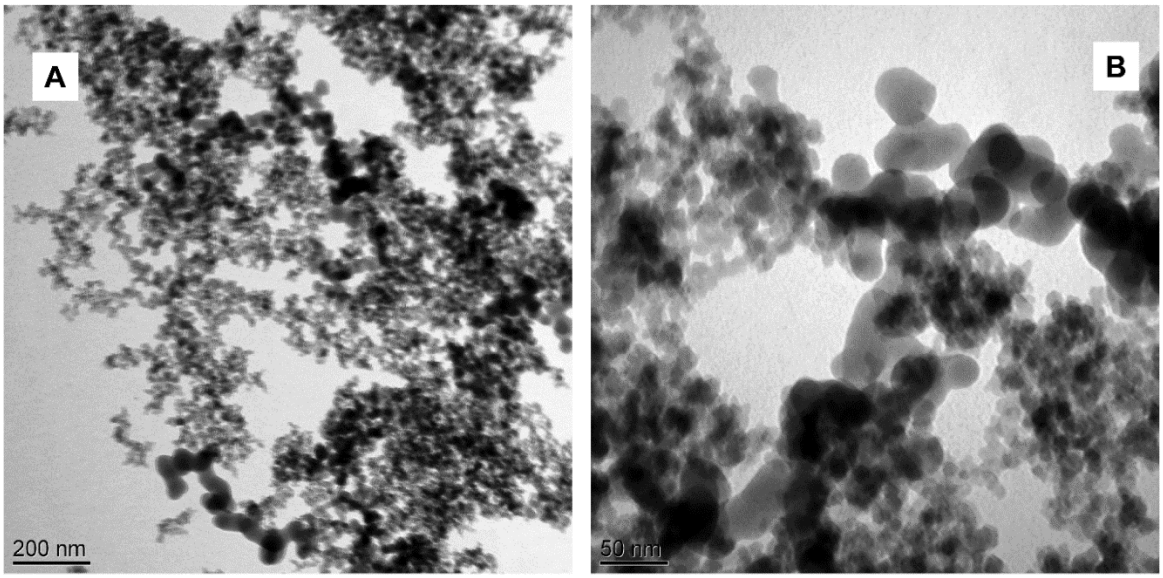

Figure 3. TEM images of SiO_2@LMAC_2MIP-3.

In conclusion, a series of MIPs were prepared using various monomers, cross-linkers, and template/monomer/cross-linker molar ratios that allow investigating the influence of molecular parameters and adjusting the proportions of these components for the manufacture of imprinted methacrylic polymer materials.

3.2. Adsorption of mitotane on imprinted materials

3.2.1. Adsorption performance of materials

Each chemical employed in the pre-polymerization mixture plays an important role in imprinting the materials surface. The formation of recognition sites depends not only on interaction forces between the template and the functional monomers in the pre-polymerization medium but also on the use of an adequate type and amount of cross-linker that maintains a good stability and strength for this template-monomer complex. These parameters may influence the specificity and density of molecular imprints, and also the non-specific adsorption properties. Indeed, specificity may be improved either by increasing the specific adsorption or by decreasing the non-specific adsorption. The evaluation of materials was carried out by

adsorption tests to determine the adsorption capacity of each imprinted material as well as its non-imprinted analog. In all the experiments, the adsorption performance for mitotane was significantly larger for the MIP than the NIP (Table S2 and Figure 4), demonstrating the formation of molecular imprints in the MIPs. The selectivity of the MIP with respect to the NIP was expressed by the "imprinting factor", *IF*, defined as

$$IF = \frac{Q(\mathrm{MIP})}{Q(\mathrm{NIP})} \quad (3)$$

All the imprinting factors were larger than one. As example, the adsorbed amount of mitotane after 15 min exposure of the MIPs prepared using LMA as monomer and either C2 or C6 cross-linker reached high values of the order of 85 % of the initial amount of mitotane (10 mL at 7.5 10^{-5} mol·L^{-1}) contacted with the adsorbent, whereas the adsorption amounts to their NIP analogs did not exceed 50 % after the same exposure time.

Three series of materials were studied for their adsorption capacities. In the first one, the types of monomer and cross-linker were varied, while keeping their amounts constant (six first rows in Table S1 and Table S2). Definite differences of adsorption capacity were noticed for each material; the highest adsorptions and *IF* were observed for materials with LMA monomer, SiO_2@LMAC_2MIP-1 and SiO_2@LMAC_6MIP-1. The highest *IF* value exhibited by LMA polymers was expected and surprising at the same time. In fact, LMA has the longest alkyl chain among the selected acrylic monomers, which strengthens the hydrophobic character of the monomer and the hydrophobic interactions with Mit [39]. On the other hand, the length of the alkyl chain affects the flexibility of the polymer. This flexibility turns the material softer, possibly in the rubber state, which may cause the loss of molecular imprints once the template is removed. The high softness of poly(lauryl methacrylate) is revealed by its low glass transition temperature (−65 °C) [40]. However, the obtained results show that the strength of interactions with the template had a higher impact than the rigidity for the formation of molecular imprints.

Indeed, the stronger interactions between the monomer and the template cause more associations between them and more possible molecular imprints. Even though part of the molecular imprints may be lost during the extraction of the template because of the polymer softness, the final balance appears being a gain of the density of effective molecular imprints.

In the second study, the effect of LMA concentration on adsorption capacity and *IF* values was investigated, only lauryl methacrylate has been used for the preparation of imprinted materials and its amount was varied from 50 mmol·L^{-1} to 160 mmol·L^{-1} (Table S2 and Figure 4B) while keeping the monomer/cross-linker ratio at 1/1. Slight improvements of MIP adsorption capacities and *IF* values were observed for both cross-linkers. Increasing the concentration of the functional monomer in the polymerization recipe shifts the association equilibrium of Mit and monomer towards higher formation of the complex species. This may lead to higher density of molecular imprints [41].

In the third study, the adsorption capability of MIPs depending on the amount of cross-linker was evaluated by increasing the concentrations of both cross-linkers from 100 mmol·L^{-1} to 320 mmol·L^{-1} while keeping constant the concentration of LMA (160 mmol·L^{-1}) (last six rows in Table S1, and Table S2 and Figure 4C). The amount of cross-linker in the polymerization reaction may affect the performance of MIPs i.e. the low amount of cross-linker may decrease the adsorption capacity and the high amount of cross-linker may lower the flexibility, decrease the mechanical stability of MIPs and make the accessibility of imprinted sites worse [42,43]. The adsorption of Mit on MIPs slightly increased from 82 % to 91 % using EGDMA as cross-linker and from 83 % to 92 % for HDDMA as cross-linker. The highest amounts of cross-linker led to adsorbed amounts approaching 90 % of the solution content, which a good result regarding a possible application to SPE devices. The highest *IF* was achieved with EGDMA as a cross-linker, namely with the SiO_2@LMAC_2MIP-3 material. EGDMA as cross-linker allows keeping a larger number of specific cavities compared to HDDMA. Indeed, the longer

polymethylene chain of HDDMA creates more flexible cross-linkages than EGDMA, resulting in loss of more molecular imprint during washing off the template. As consequence, the best imprinted polymer among the prepared series is SiO_2@LMAC$_2$MIP-3 due to its highest *IF* value (2.4) and its important adsorption (87.5 %).

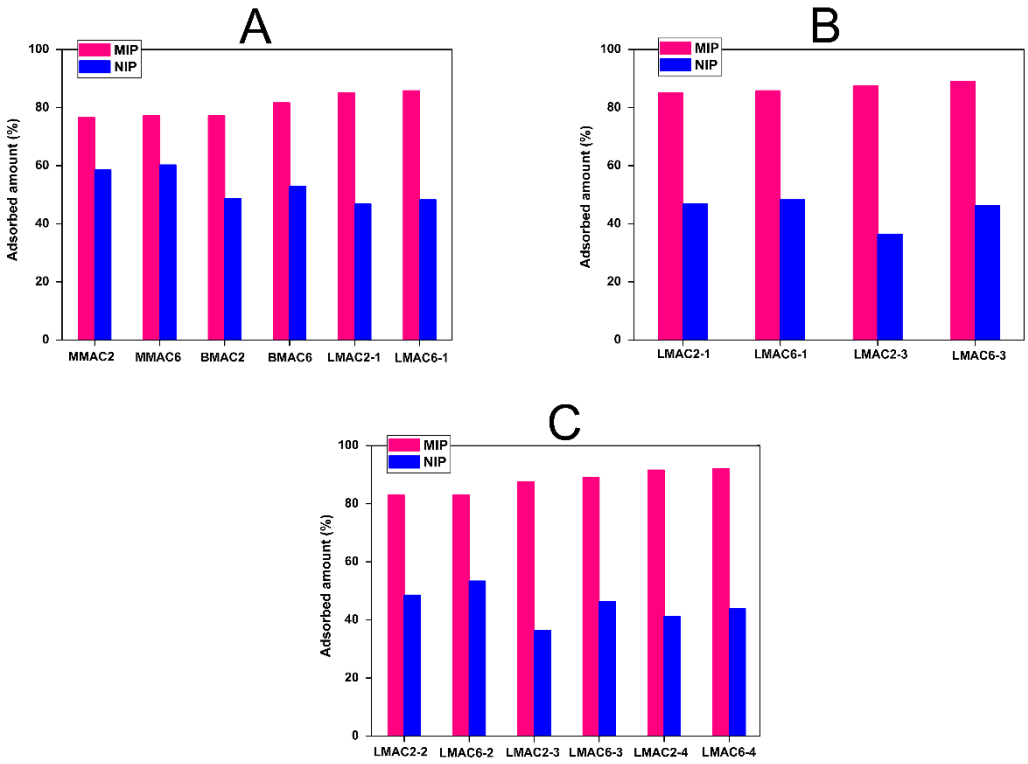

Figure 4. Influence of monomer type (A), monomer concentration (B), and cross-linker concentration (C) on the adsorption capacities of mitotane onto imprinted materials at 25 °C, solution volume = 10 mL, [Mit] = 7.5 10^{-5} mol·L^{-1} in a mixture of water/methanol (50/50) (v/v), contact time = 15 min.

As a summary, it is possible to design MIP materials relying on hydrophobic interactions with the analyte. Though hydrophobic interactions are presumed non-specific, a highly hydrophobic monomer is preferable. This criterion for the choice of the monomer is a better relevance than the rigidity of the resulting polymer ensuring freezing of molecular imprints.

3.2.2. Thermodynamics of adsorption

Thermodynamics of adsorption have been investigated through adsorption isotherms presenting the relationship between adsorbed amount and residual concentration in solution at equilibrium. They have been measured by the depletion method. The experimental adsorption isotherms were interpreted with the help of thermodynamic models. The first approach makes use of the Scatchard model [44]. The Scatchard plot is a linearized representation of the Langmuir adsorption isotherm that writes as Eq. 4 in the case of homogeneous and independent binding sites.

$$\frac{Q}{C} = -KQ + KQ_{max} \quad (4)$$

where Q is the adsorbed amount (mol·m^{-2}), K is the adsorption equilibrium constant, and Q_{max} is the maximum adsorbed amount corresponding to full occupancy of adsorption sites reached at high concentrations of solute. So, the plot of Q/C as a function of Q is linear when the assumptions of the Scatchard theory are met, and its negative slope gives the binding equilibrium constant K.

The Scatchard plot for MIP shown in Figure 5 presents two distinct parts of linear behavior with two different distinct slopes, implying two kinds of non-equivalent binding sites with different affinities. Conversely, the Scatchard plot for NIP displayed a single linear behavior over the whole Q range, which indicated adsorption to only one type of binding site (Figure 5). Scatchard plots of experimental data of the MIP and NIP materials in are too much scattered to allow accurate calculations of binding constants and Q_{max}. Scatchard plots just gave evidence of the existence of two kinds of binding sites for the MIP and only one kind of binding site for the NIP [29].

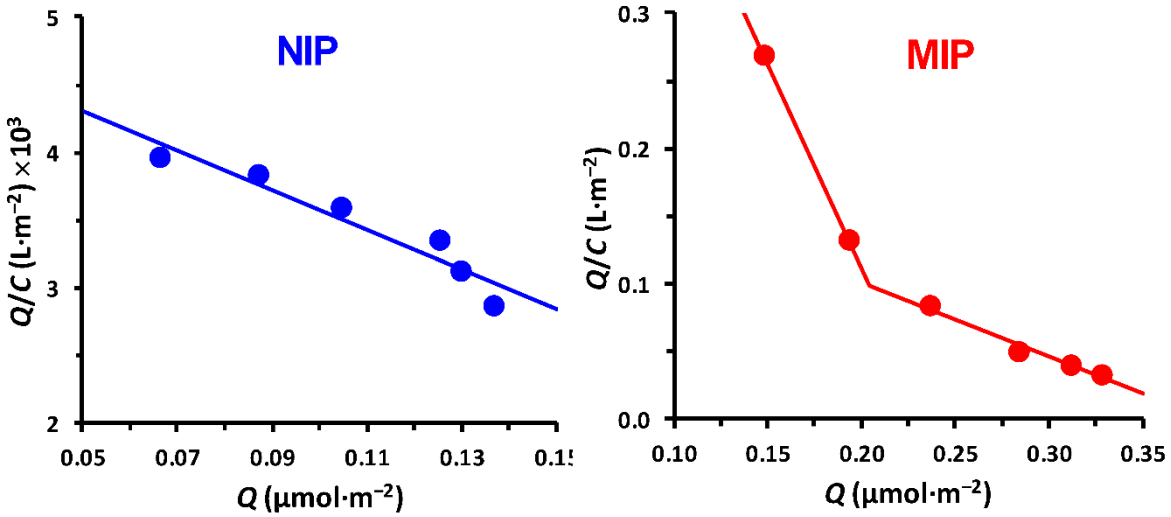

Figure 5. Scatchard plots for binding data of mitotane onto SiO_2@LMAC_2NIP-3 (left) and SiO_2@LMAC_2MIP-3 (right).

The Scatchard model and its underlying Langmuir model consider adsorption to binding sites. The concept of "binding site" does not correspond to reality however. Indeed, molecular imprints have the features of well-defined binding sites where mitotane molecules adsorb and stay there. The Langmuir theory describes monolayer adsorption on a homogeneous surface containing a well-defined number of independent binding sites where adsorbate molecules adsorb with no interaction with each other [45]. Adsorption at the materials surface offside the molecular imprints does not take place on binding sites. For the LMA-based materials, hydrophobic interactions with the layer of *n*-dodecyl chains are mainly responsible for the adsorption. Adsorbed molecules are mobile and diffuse laterally on the surface. The assumptions of the Langmuir model are not valid for mobile adsorbed molecules [46,47]. The simplest model for adsorption of mobile molecules as a monolayer is the Volmer isotherm [48]. The relevant thermodynamic model is a combination of adsorption on molecular imprints considered as specific sites and non-specific adsorption as a mobile layer. Such thermodynamic approach has recently been introduced as the Langmuir−Volmer model [29]. So, the adsorption on NIPs was modelled using the Volmer adsorption isotherm and adsorption on MIPs was

modelled using the Langmuir−Volmer adsorption isotherm. The widely used Langmuir and bi-Langmuir models may fit quite well the experimental data. They are quite popular because of the simplicity of their mathematical expressions [49,50]. The Volmer and Langmuir models generally fit the experimental data equally well [29]. The fit of the Langmuir isotherm to the NIP data is not so good, as revealed by the poor match of experimental data to a linear behavior in the Scatchard plot. Mobile adsorption isotherms are preferred for the non-specific adsorption because they correspond to the known physical chemistry of adsorption.

For localized adsorption on the specific sites of molecular imprints of MIP, the adsorbed amount Q_S (mol·m^{-2}) at equilibrium is related to the maximum adsorption capacity $Q_{max,S}$, the equilibrium concentration C (mol·L^{-1}) and the adsorption equilibrium constant K_S by the Langmuir equation:

$$Q_S = Q_{max,S}\frac{K_S C}{1+K_S C} \quad (5)$$

For non-specific adsorption on NIP and at the MIP surface off its molecular imprints, the Volmer isotherm was considered.

$$C = \frac{1}{K_{NS}}\frac{\theta}{1-\theta}e^{\frac{\theta}{1-\theta}} \quad (6)$$

where $\theta = Q_{NS}/Q_{max,NS}$ is the surface coverage. It is written as C being a functional of Q_{NS}, i.e. $C(Q_{NS}, Q_{max,NS}, K_{NS})$; it has been inverted into Q_{NS} as a function of C by means of numerical resolution of Eq. 6. The theoretical adsorption models were fitted to experimental data so as to obtain adsorption parameters of mitotane onto the MIP and NIP materials. Fitting the models to experimental data was achieved by minimization of the average relative error function (*ARE*):

$$ARE = \frac{1}{n-p}\sum_{i=1}^{n}\left|\frac{Q_{exp}-Q_{calc}}{Q_{exp}}\right| \quad (7)$$

where n and p is the number of data points and fitted parameters respectively, Q_{exp} and Q_{calc} are the experimental and fitted the adsorbed amounts at equilibrium respectively. Adsorption to the NIP is described by the two parameters of the Volmer isotherm, $Q_{max,NS}$ and K_{NS}. Adsorption

to the MIP is described by the four parameters of the Volmer isotherm for non-specific adsorption, $Q_{max,NS}$ and K_{NS}, and Langmuir isotherm for specific adsorption on molecular imprints, $Q_{max,S}$ and K_S. The total adsorbed amount measured in adsorption experiments is the sum of the two contributions, $Q_{max,S} + Q_{max,NS}$.

The Volmer and Langmuir–Volmer models fitted the respective experimental adsorption isotherms of SiO_2@LMAC_2NIP-3 and SiO_2@LMAC_2MIP-3 with high accuracy (Figure 6). The thermodynamic parameters and average relative error (*ARE*) values are given in Table 1.

The main outcomes are the following. The density of selective binding sites is quite high as it represents 1/3 of the maximum density of adsorbed Mit. The total maximum adsorbed amounts of Mit to MIP and NIP is the same. The large ratio of equilibrium constants K_S(MIP)/K_{NS}(NIP) ≈ 500 shows the much higher affinity to molecular imprints than to the non-imprinted material. The equilibrium constants for non-specific adsorption to the MIP and NIP are quite different (K_{NS}(MIP)/K_{NS}(NIP) ≈ 10). The analysis of adsorption isotherms clearly showed that there were two distinct adsorption processes. They were ascribed to adsorption to molecular imprints and off the molecular imprints for the high affinity and low affinity processes respectively. However, the adsorption to the MIP off the molecular imprints is stronger than the adsorption to the NIP. As a tentative explanation, the low affinity part of adsorption to the MIP may occur to molecular imprints that have been damaged during the extraction of the template at the last step of the synthesis process. Indeed, the softness of the LMA-based polymer is detrimental to keeping the molecular imprints upon washing off the template. It is presumed that part of the molecular imprints were kept thanks to the cross-linkages (1/3 of the total) and the remainder has been lost during extraction of the template.

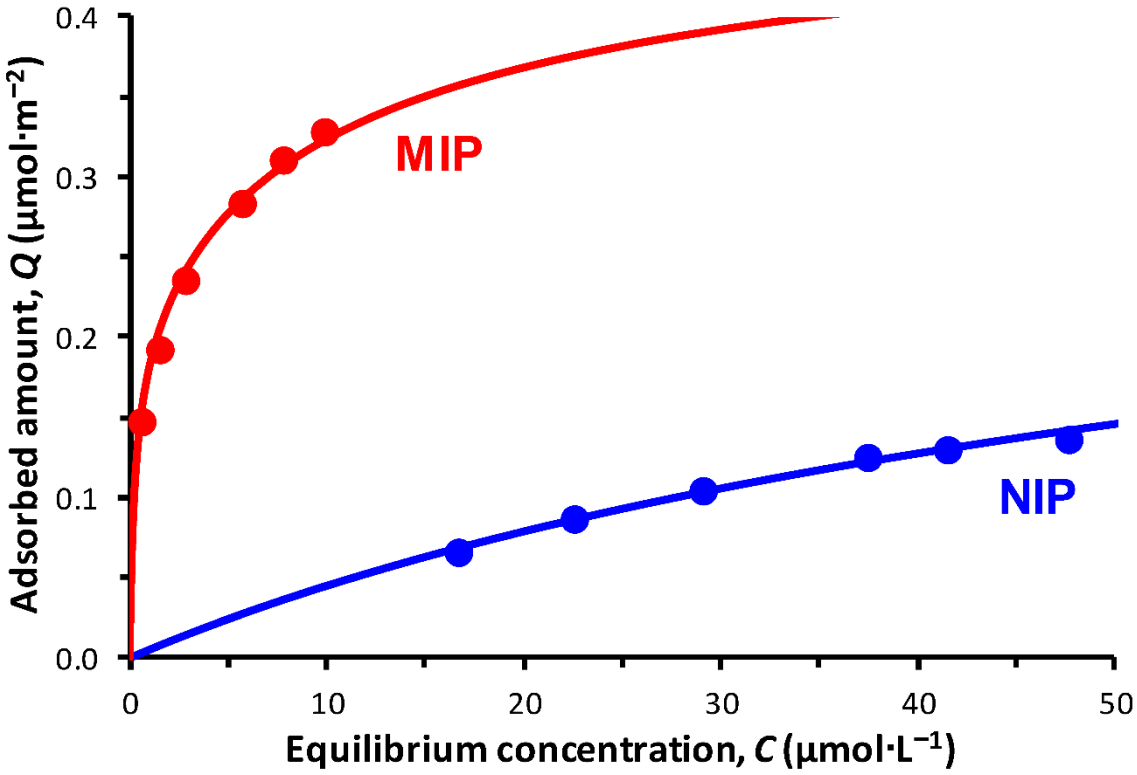

Figure 6. Experimental adsorption isotherms and best non-linear fits of the adsorption models for adsorption of mitotane to SiO_2@LMAC_2NIP-3 and SiO_2@LMAC_2MIP-3.

Table 1. Parameters of the best fits of the Volmer and Volmer–Langmuir models to experimental adsorption isotherms of mitotane onto NIP and MIP materials at 298 K.

	Non-selective adsorption		Selective adsorption		
	$Q_{max,NS}$ (µmol·m^{-2})	log(K_{NS})	$Q_{max,S}$ (µmol·m^{-2})	log(K_S)	*ARE*
SiO_2@LMAC_2NIP-3 (Volmer)	0.61	3.93	–	–	0.030
SiO_2@LMAC_2MIP-3 (Volmer–Langmuir)	0.42	4.90	0.19	6.60	0.063

Adsorption isotherms at different temperatures (Figure 7A) allow determining the enthalpic and entropic contributions to the adsorption process. Increasing temperature from 298 K to 328 K led to a decrease in the retention of mitotane for the two types of binding sites, suggesting that the binding processes were exothermic.

A significant decrease of affinity of mitotane for low energy binding sites from K_{NS} = 8.0 10^4 to K_{NS} = 2.7 10^4, and for high energy binding sites from K_S = 4.0 10^6 to K_S = 1.5 10^6 were observed upon increasing the temperature (Table 2).

Table 2. Fitted parameters of the Langmuir–Volmer model to experimental adsorption isotherms of mitotane onto SiO_2@LMAC$_2$MIP-3 at different temperatures.

	Non-selective adsorption		Selective adsorption	
Temperature (K)	$Q_{max,NS}$ (µmol·m^{-2})	log(K_{NS})	$Q_{max,S}$ (µmol·m^{-2})	log(K_S)
298	0.421	4.90	0.190	6.60
308	0.421	4.72	0.190	6.43
318	0.421	4.64	0.190	6.20
328	0.421	4.43	0.190	6.18

The standard Gibbs free energy of adsorption $\Delta_{ads}G^0$, standard enthalpy $\Delta_{ads}H^0$ and standard entropy $\Delta_{ads}S^0$ were calculated from the binding constants K_i (K_S and K_{NS}) and their dependence on temperature using the Gibbs and van't Hoff equations for each type of binding process:

$$\Delta_{ads}G_i^0 = -RT\ln(K_i) \quad (8)$$

$$\Delta_{ads}G_i^0 = \Delta_{ads}H_i^0 - T\,\Delta_{ads}S_i^0 \quad (9)$$

Combination of the two equations yields the van't Hoff equation:

$$\ln(K_i) = \frac{\Delta_{ads}S_i^0}{R} - \frac{\Delta_{ads}H_i^0}{RT} \quad (10)$$

where R (8.314 J·mol^{-1}·K^{-1}) is the gas constant and T (K) is the absolute temperature. The values standard enthalpy ($\Delta_{ads}H_i^0$) and standard entropy ($\Delta_{ads}S_i^0$) were determined from the slope and *y*-intercept of the plot of Log(K_i) vs 1/T.

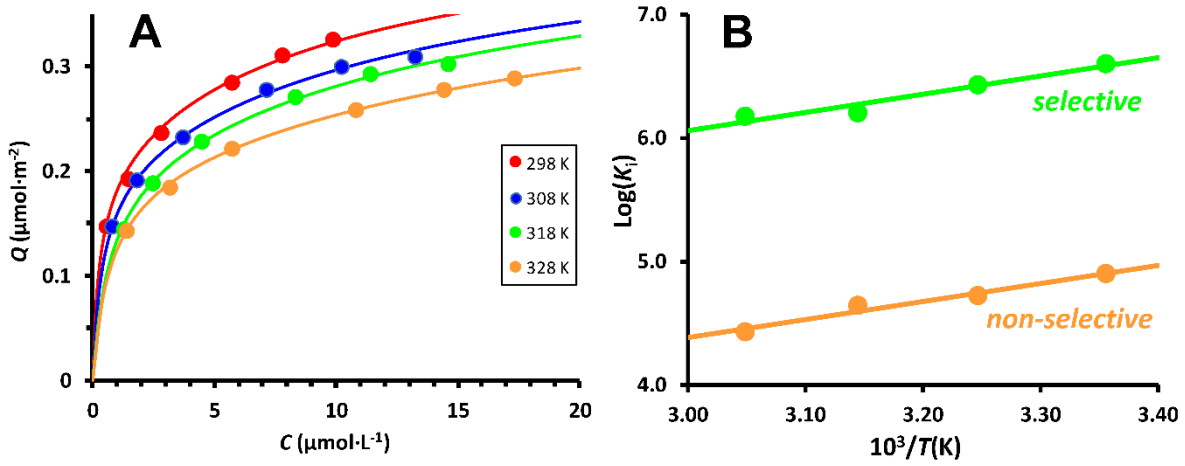

Figure 7. (A) Adsorption isotherms of mitotane onto SiO_2@LMAC$_2$MIP-3 at different temperatures. (B): van't Hoff plot of the binding constant of mitotane onto SiO_2@LMAC$_2$MIP-3 against inverse temperature.

The van't Hoff plots of Figure 7B are linear, showing that their analysis in terms of temperature-independent values of $\Delta_{ads}H^0$ and $\Delta_{ads}S^0$ is valid. These values were $\Delta_{ads}H_S^0 = -28.3$ kJ·mol^{-1} and $\Delta_{ads}S_S^0 = 31.1$ kJ·mol^{-1}·K^{-1} for the adsorption to molecular imprints, and $\Delta_{ads}H_S^0 = -27.9$ kJ·mol^{-1} and $\Delta_{ads}S_S^0 = 0.13$ kJ·mol^{-1}·K^{-1} for the adsorption off the molecular imprints. The standard free enthalpy values $\Delta_{ads}G^0$ for both sites are negative, indicating that the adsorption processes are spontaneous onto the two types of binding sites within the tested temperature range. The negative value of $\Delta_{ads}H^0$ for both sites confirms that the adsorption process is exothermic. The large increase of entropy upon the specific adsorption process may correspond to the release of water molecules that were frozen in contact to the polymer surface inside the "cavity" of molecular imprints. Such entropy variation vanishes for non-specific adsorption because the adsorbed Mit molecules are mobile in the layer of alkyl chains of the polymer surface. The different values of $\Delta_{ads}S_S^0$ for specific and non-specific adsorption is an experimental clue for adsorption to molecular imprints is localized (modeled by the Langmuir isotherm) and that off molecular imprints is mobile (modeled by the Volmer isotherm).

3.2.3. Kinetics of adsorption

The effect of contact time on mitotane adsorption onto the SiO_2@LMAC_2MIP-3 and SiO_2@LMAC_2NIP-3 materials was investigated for several mitotane concentrations (Figure 8). All kinetic curves showed that by increasing the contact time, the adsorbed amount of mitotane increased. Similar finding was reported showing the same shape of kinetic plot [51]. The amount of mitotane retained by the SiO_2@LMAC_2MIP-3 is much greater than that retained by the SiO_2@LMAC_2NIP-3 in the whole tested mitotane concentration range and during the full contact time. Adsorption equilibrium was reached within 15 min. Adsorption of SiO_2@LMAC_2MIP-3 was quite fast as more than 70 % of equilibrium adsorption was reached within the first few minutes. This shows one advantage of imprinted materials coated as thin films at the surface of a porous solid support. Indeed, materials prepared by traditional bulk polymerization often need 1–10 h to reach adsorption equilibrium [11,29,52]. Optimization of material porosity and extraction conditions in SPE cartridges may improve kinetic performances [53]. Therefore, the present fast adsorption kinetics came from the favorable porosity of the solid support and the thin thickness of the MIP layer.

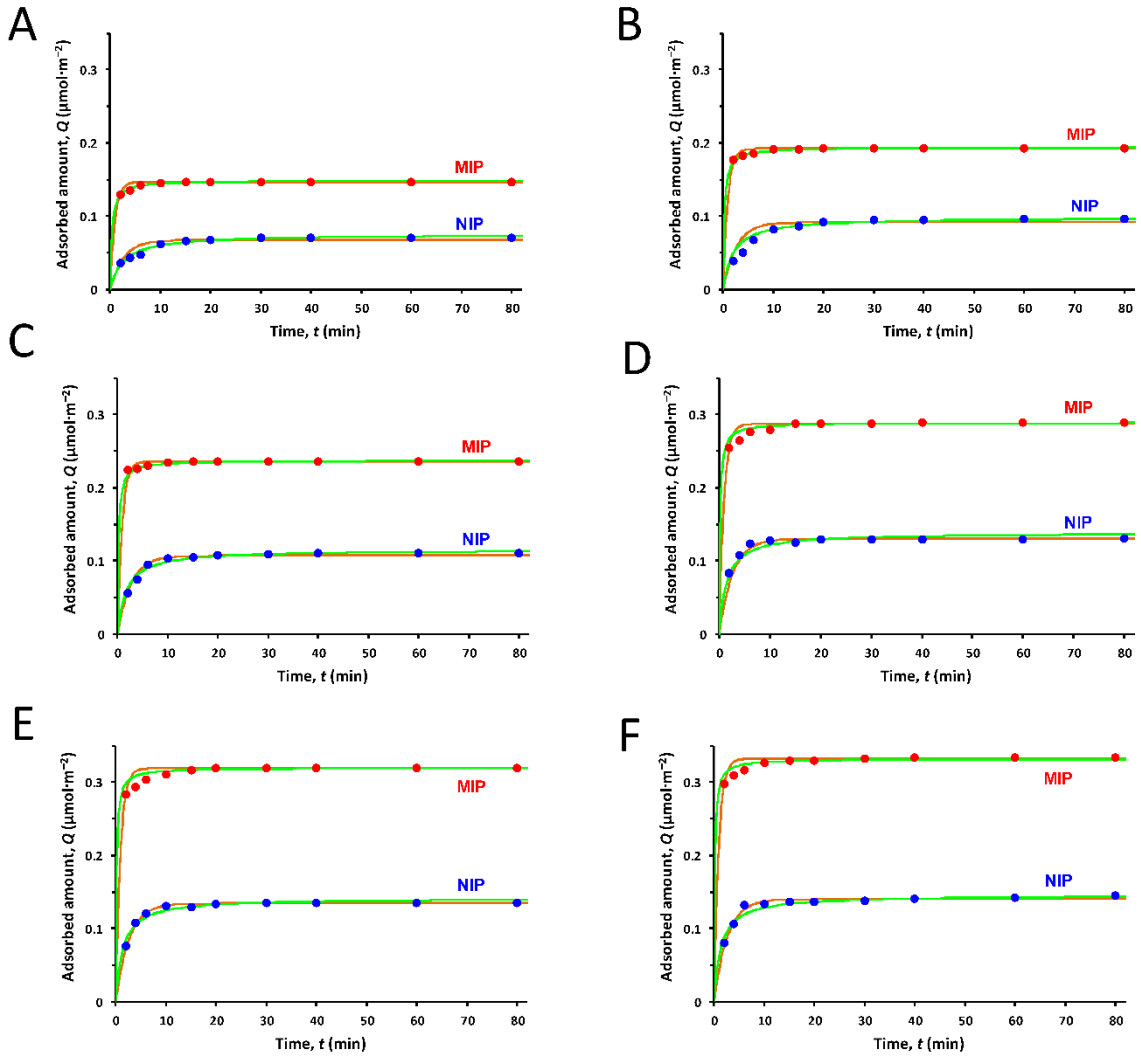

Figure 8. Experimental adsorption kinetics and nonlinear fits of the pseudo-first-order (red lines) and pseudo-second-order (green lines) models for respective adsorption of mitotane to SiO_2@LMAC$_2$MIP-3 and SiO_2@LMAC$_2$NIP-3 at initial concentration (A): 7.5 10^{-5} mol·L^{-1}, (B): 7 10^{-5} mol·L^{-1}, (C): 6.25 10^{-5} mol·L^{-1}, (D): 5 10^{-5} mol·L^{-1}, (E): 4 10^{-5} mol·L^{-1}, (F): 3 10^{-5} mol·L^{-1}.

Kinetic models have been compared to the experimental data of SiO_2@LMAC$_2$MIP-3 and SiO_2@LMAC$_2$NIP-3. Pseudo-first-order [54] and pseudo-second-order [55] models have been commonly used to assess the adsorption mechanism.

The pseudo-first order model, established by Lagergren, describes the adsorption kinetics where the rate is first-order with respect to the surface concentration of available adsorption sites [56].

The adsorption rate at time t is proportional to the difference between the amount adsorbed at equilibrium $Q(\infty)$ and the amount adsorbed at time t, $Q(t)$:

$$\frac{dQ(t)}{dt} = k_1[Q(\infty) - Q(t)] \quad (11)$$

Integration using $Q(0) = 0$ gives:

$$Q(t) = Q(\infty)[1 - e^{-k_1 t}] \quad (12)$$

where k_1 (min^{-1}) is the kinetic constant of pseudo-first order, and $Q(t)$ and $Q(\infty)$ are the adsorbed amounts at a given time t and at equilibrium.

The non-linear form of the pseudo-second-order adsorption rate equation, established by Blanchard [57], is often successfully used to describe the kinetics of the binding reaction of metal ions to solid supports [55,58]. It reads

$$\frac{dQ(t)}{dt} = k_2[Q(\infty) - Q(t)]^2 \quad (13)$$

Integration using $Q(0) = 0$ yields

$$Q(t) = \frac{k_2 Q(\infty)^2 t}{1 + k_2 Q(\infty) t} \quad (14)$$

where k_2 ($m^2 \cdot \mu mol^{-1} \cdot min^{-1}$) is the kinetic constant of pseudo-second order and $Q(t)$ and $Q(\infty)$ are the adsorbed amounts at a given time t and at equilibrium.

The pseudo-first order and the pseudo-second-order models were fitted to experimental data by minimizing the average relative error (*ARE*). Both kinetic models fitted rather closely experimental data, the pseudo-second-order model providing a better account for the experiments (Figure 8). It was difficult to discriminate the validity of the two models however. This lack of sensitivity came from the experimental dataset that was rather close to equilibrium, even for the shortest times possible under the experimental conditions. The adsorption kinetics were too fast for their measurement could be performed at their early stages. The fitted adsorbed amounts at equilibrium corresponded quite nicely to the equilibrium values measured after a very long adsorption time, which was expected since the time scale of experimental data was

long enough for reaching equilibrium. The rate constants of the pseudo-first order model were k_1 = 1.1 min^{-1} (*ARE* = 0.014) for the MIP and k_1 = 0.38 min^{-1} (*ARE* = 0.046) for the NIP. The rate constants of the pseudo-second order model were k_2 = 21.3 $m^2 \cdot mol^{-1} \cdot min^{-1}$ (*ARE* = 0.01) for the MIP and k_2 = 5.1 $m^2 \cdot mol^{-1} \cdot min^{-1}$ (*ARE* = 0.04) for the NIP. Whatever the model, adsorption to the MIP was about 3–4 times faster than to the NIP. The faster adsorption to the molecular imprints was presumably due to their high availability on the thin polymer layer coating the porous solid support. At variance with the present results, faster adsorption for the NIP has been observed for adsorption of the λ-cyhalothrin insecticide onto a macroporous MIP prepared by polymerization of a concentrated W/O Pickering emulsions stabilized by magnetic Fe_3O_4 nanoparticles (high internal phase emulsions, HIPEs) [59]. The availability of the molecular imprints appears a key parameter for controlling the adsorption kinetics.

3.3. Selectivity

The evaluation of the adsorption selectivity of the MIPs allows identifying the recognition efficiency of imprinted polymers for the target in the presence of other interferents having a similar structure. The adsorption of the target molecule is compared to the adsorption of interfering molecules under the same conditions. In order to validate the selectivity of the imprinted polymer SiO_2@LMAC_2MIP-3 for Mit, three potential competitor agents, *p,p′*-dichlorodiphenyldichloroethene, chlorpyrifos and endosulfan were selected for selectivity experiments because these organochlorine products could be found as competitive pollutants in the loaded matrix such as ground water and soil. The competing molecules are related to Mit in terms of structural similarity and their high frequency of occurrence with mitotane (Figure 9). The adsorbed amounts of Mit, *p,p′*-dichlorodiphenyldichloroethene, chlorpyrifos and endosulfan onto SiO_2@LMAC2NIP-3 or SiO_2@LMAC2MIP-3 adsorbents were separately determined for a single concentration of each solution using UV-Vis spectroscopy similarly as

for Mit. Experimental results (Table 3) show the characteristic parameters, including distribution coefficients and selectivity coefficients.

The distribution coefficient (D, L·g^{-1}) corresponding to the partition of the substrate between the MIP and the solution was defined as:

$$D = \frac{Q_e}{C_e} \quad (15)$$

where Qe (mg·g^{-1}) is the adsorption capacity at equilibrium and Ce (mg·L^{-1}) is the equilibrium concentration of molecules. The ratio of the distribution coefficients gives a selectivity coefficient α (Eq. 16) for the three of interfering molecules under consideration.

$$\alpha = \frac{D_{\text{analyte,MIP}}}{D_{\text{competitor,MIP}}} \quad (16)$$

where $D_{\text{analyte,MIP}}$ and $D_{\text{competitor,MIP}}$ are the distribution coefficients for the template molecule and for the competitive molecules respectively.

SiO_2@LMAC_2MIP-3 has higher extraction efficiency of Mit than its structural analogues. In addition, a comparison of the extraction efficiency of the imprinted and non-imprinted polymers for each compound indicates that SiO_2@LMAC_2MIP-3 has a higher selectivity for Mit molecules. The distribution ratio of SiO_2@LMAC_2MIP-3 towards Mit was evidently higher than the distribution ratios of interfering molecules. This suggests that the migration of Mit to specific binding sites of the imprinted polymer is more favorable, resulting in a more favorable adsorption of Mit compared to its structural analogs [60]. In the case of SiO_2@LMAC_2MIP-3, the values of selectivity coefficient α with respect to Mit were high. Such results provide a definite demonstration of the highly selective recognition of the imprinted polymer towards Mit indicating that the imprinted cavities created by the template are not able to accommodate *p,p′*-dichlorodiphenyldichloroethene, chlorpyrifos and endosulfan may be due to molecular size, and the memory of specific structure. The polymer-template interaction created during the preparation of the MIP involves the hydrophobic interactions between the alkyl chains and

chlorine atoms of Mit that play an important role in the recognition of the template molecules. All these results clearly revealed that MIP can be selected as a promising adsorbent, which exhibited good recognition selectivity and binding affinity for Mit molecules that are suitable for SPE technique to extract selectively Mit from complex matrices in media.

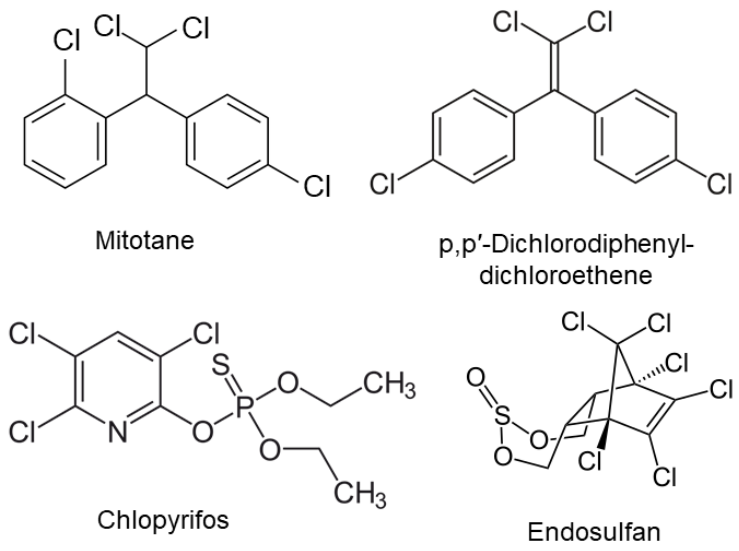

Figure 9. Chemical structures of Mitotane and the interfering molecules.

Table 3. Adsorption of Mit and competitive interfering compounds of SiO_2@LMAC_2MIP-3 and SiO_2@LMAC_2NIP-3.

Molecules	SiO_2@LMAC_2NIP-3			SiO_2@LMAC_2MIP-3		
	Extraction efficiencies (%)	D ($L \cdot g^{-1}$)	α	Extraction efficiencies (%)	D ($L \cdot g^{-1}$)	α
Mitotane	57.61	1.35	–	98.18	54.10	–
p,p′-Dichlorodiphenyl-dichloroethene	56.02	1.27	1.067	88.04	7.36	7.34
Chlorpyrifos	58.02	1.38	0.98	76.03	3.17	17.05
Endosulfan	59.01	1.43	0.94	62.08	1.63	33.05

4. Conclusion

To sum up, a series of imprinted and non-imprinted polymers were successfully synthesized on the surface of silica covered with 3-mercaptopropyl groups by means of a radical transfer

reaction with the use of functional monomers and cross-linking agents of variable hydrophobic character to select the optimum synthesis conditions for MIP preparation. The recognition propriety of the prepared MIPs towards mitotane was evaluated by adsorption process. The highest *IF* value (2.4) which demonstrates the formation of specific sites on MIP surface was exhibited by SiO_2@LMAC_2MIP-3 (with a high adsorption capacity: 21 $mg \cdot g^{-1}$) prepared by the most hydrophobic pair of monomer and cross-linker. This suggests that the molecular imprints were generated as the template molecules were washed off on the basis of the hydrophobic interactions between the target molecule and the functional monomer used in MIP preparation. The adsorption isotherms of NIP and MIP materials were closely accounted for by the Volmer and Langmuir–Volmer models instead of the popular models used in literature. The thermodynamic parameters $\Delta_{ads}G^0$, $\Delta_{ads}H^0$ and $\Delta_{ads}S^0$ reveal that the adsorption on the MIP is spontaneous, exothermic for both selective and non-selective binding. The kinetic study for SiO_2@LMAC_2MIP-3 showed a fast behavior by reaching equilibrium within 15 min. In selectivity trial, the extraction efficiency of SiO_2@LMAC_2MIP-3 towards mitotane was 98.2 % higher than those obtained towards its competitors such as 62 % for endosulfan molecules. These good performances of SiO_2@LMAC_2MIP-3 such as fast adsorption and high adsorption efficiency for mitotane make this material a promising adsorbent in SPE method to extract mitotane from aqueous media and also it is interesting to test its performances in blood media.

Acknowledgements

This work was supported by funding from the “Partenariat Hubert CurienUtique” for French-Tunisian cooperation, grant n° 19G1204.

References

[1] B. Sellergren (Ed.), Molecularly Imprinted Polymers. Man-made Mimics of Antibodies and their Applications in Analytical Chemistry. Elsevier, Amsterdam (2001).

[2] C. Alvarez-Lorenzo, A. Concheiro (Eds.), Handbook of Molecularly Imprinted Polymers. SmithersRapra, Shawbury, UK (2013).

[3] L.M. Madikizela, P.S. Mdluli, L. Chimuka, Experimental and theoretical study of molecular interactions between 2-vinyl pyridine and acidic pharmaceuticals used as multi-template molecules in molecularly imprinted polymer. React. Funct. Polym. 103 (2016) 33–43. doi:10.1016/j.reactfunctpolym.2016.03.017.

[4] L.E. Gómez-Pineda, G.E. Pina-Luis, Á. Cuán, J.A. García-Calzón, M.E. Díaz-García, Physico-chemical characterization of flavonol molecularly imprinted polymers. React. Funct. Polym. 71 (2011) 402–408. doi:10.1016/j.reactfunctpolym.2010.12.013.

[5] N. Martins, E.P. Carreiro, M. Simões, M.J. Cabrita, A.J. Burke, R. Garcia, An emerging approach for the targeting analysis of dimethoate in olive oil: The role of molecularly imprinted polymers based on photo-iniferter induced ‘‘living’’ radical polymerization. React. Funct. Polym. 86 (2015) 37–46. doi:10.1016/j.reactfunctpolym.2014.11.003.

[6] A. Anene, R. Kalfat, Y. Chevalier, S. Hbaieb, Molecularly imprinted polymer-based materials as thin films on silica supports for efficient adsorption of Patulin. Colloids Surf. A: Physicochem. Eng. Asp. 497 (2016) 293–303. doi:10.1016/j.colsurfa.2016.03.005.

[7] A. Anene, R. Kalfat, Y. Chevalier, S. Hbaieb, Design of molecularly imprinted polymeric materials: The crucial choice of functional monomers. Chemistry Africa 3 (2020) 769–781. doi:10.1007/s42250-020-00180-1.

[8] V.D. Salian, C.J. White, M.E. Byrne, Molecularly imprinted polymers via living radical polymerization: Relating increased structural homogeneity to improved template binding parameters. React. Funct. Polym. 78 (2014) 38–46. doi:10.1016/j.reactfunctpolym.2014.02.003.

[9] M. Bitar, J. Maalouly, H. Chebib, A. Lerbret, P. Cayot, E. Bou-Maroun, Experimental design approach in the synthesis of molecularly imprinted polymers specific for iprodione fungicide. React. Funct. Polym. 94 (2015) 17–24. doi:10.1016/j.reactfunctpolym.2015.07.002.

[10] S. Hussain, S. Khan, S. Gul, M.I. Pividori, M.D.P.T. Sotomayor, A novel core@shell magnetic molecular imprinted nanoparticles for selective determination of folic acid in different food samples. React. Funct. Polym. 106 (2016) 51–56. doi:10.1016/j.reactfunctpolym.2016.07.011.

[11] A. Wong, F.M. de Oliveira, C.R.T. Tarley, M.D.P.T. Sotomayor, Study on the cross-linked molecularly imprinted poly(methacrylic acid) and poly(acrylic acid) towards selective adsorption of diuron. React. Funct. Polym. 100 (2016) 26–36. doi:10.1016/j.reactfunctpolym.2016.01.006.

[12] C. Cueto, J.H.U. Brown, The chemical fractionation of an adrenocorticolytic drug. Endocrinology 62 (1958) 326–333. doi:10.1210/endo-62-3-326.

[13] V. Turusov, V. Rakitsky, L. Tomatis, Dichlorodiphenyltrichloroethane (DDT): ubiquity, persistence, and risks. Environ. Health Perspect. 110 (2002) 125–128. doi:10.1289/ehp.02110125.

[14] M.L. Gutierrez, S.T. Crooke, Mitotane (o,p'-DDD). Cancer Treatment Rev. 7 (1980) 49–55. doi:10.1016/S0305-7372(80)80025-9.

[15] P.M. van Koetsveld, S.G. Creemers, F. Dogan, G.J.H. Franssen, W.W. de Herder, R.A. Feelders, L.J. Hofland, The efficacy of mitotane in human primary adrenocortical carcinoma cultures. J. Clin. Endocrinol. Metab. 105 **(**2020) 407–417. doi:10.1210/clinem/dgz001.

[16] R.M. Paragliola, A. Corsello, P. Locantore, G. Papi, A. Pontecorvi, S.M. Corsello, Medical approaches in adrenocortical carcinoma. Biomedicines 8 (2020) 551. doi:10.3390/biomedicines8120551.

[17] J. Miao, A. Liu, L. Wu, M. Yu, W. Wei, S. Liu, Magnetic ferro ferric oxide and polydopamine molecularly imprinted polymer nanocomposites based electrochemical impedance sensor for the selective separation and sensitive determination of dichlorodiphenyltrichloroethane (DDT). Anal. Chim. Acta, 1095 (2020) 82–92. doi: 10.1016/j.aca.2019.10.027.

[18] J. Płotka-Wasylka, N. Szczepańska, M. Guardia, J. Namieśnik, Miniaturized solid-phase extraction techniques. Trends Anal. Chem. 73 (2015) 19–38. doi:10.1016/j.trac.2015.04.026.

[19] L.M. Madikize, S. Ncube, L. Chimuka, Recent developments in selective materials for solid phase extraction. Chromatographia 82 (2019) 1171–1189. doi:10.1007/s10337-018-3644-8.

[20] A. Mornar, M. Sertić, N. Turk, B. Nigović, M. Koršić, Simultaneous analysis of mitotane and its main metabolites in human blood and urine samples by SPE-HPLC technique. Biomed. Chromatogr. 26 (2012) 1308–1314. doi:10.1002/bmc.2696.

[21] C.F. Pool, New trends in solid-phase extraction. Trends Anal. Chem. 22 (2003) 362–373. doi:10.1016/S0165-9936(03)00605-8.

[22] M. Arabi, A. Ostovan, A.R. Bagheri, X. Guo, L. Wang, J. Li, X. Wang, B. Li, L. Chen, Strategies of molecular imprinting-based solid-phase extraction prior to chromatographic analysis. Trends Anal. Chem. 128 (2020) 115923. doi:10.1016/j.trac.2020.115923.

[23] L.M. Madikizela, N.T. Tavengwa, H. Tutu, L. Chimuka, Green aspects in molecular imprinting technology: From design to environmental applications. Trends Anal. Chem. 17 (2018) 14–22. doi:10.1016/j.teac.2018.01.001.

[24] X. Song, S. Xu, L. Chen, Y. Wei, H. Xiong, Recent advances in molecularly imprinted polymers in food analysis. J. Appl. Polym. Sci. 131 (2014) 1–18.doi:10.1002/app.40766.

[25] C. Unger, P.A. Lieberzeit, Molecularly imprinted thin film surfaces in sensing: Chances and challenges. React. Funct. Polym. 161 (2021) 104855. doi:10.1016/j.reactfunctpolym.2021.104855.

[26] I. Polyakova, L. Borovikova, A. Osipenko, E. Vlasova, B. Volchek, O. Pisarev, Surface molecularly imprinted organic-inorganic polymers having affinity sites for cholesterol. React. Funct. Polym. 109 (2016) 88–98. doi:10.1016/j.reactfunctpolym.2016.10.010.

[27] C. Ayadi, A. Anene, R. Kalfat, Y. Chevalier, S. Hbaieb, Molecularly imprinted polyaniline on silica support for the selective adsorption of benzophenone-4 from aqueous media. Colloids Surf. A: Physicochem. Eng. Aspects 567 (2019) 32–42. doi:10.1016/j.colsurfa.2019.01.042.

[28] A. Anene, K. Hosni, Y. Chevalier, R. Kalfat, S. Hbaieb, Molecularly imprinted polymer for extraction of patulin in apple juice samples. Food Control 70 (2016) 90–95. doi:10.1016/j.foodcont.2016.05.042.

[29] C. Ayadi, A. Anene, R. Kalfat, Y. Chevalier, S. Hbaieb, Molecular imprints frozen by strong intermolecular interactions in place of cross-linking. Chem. Eur. J. 27 (2021) 2175–2183. doi:10.1002/chem.202004580.

[30] G. Socrates, Infrared and Raman Characteristic Group Frequencies. 3rd ed., Wiley, Chichester (2001) p. 209.

[31] Y.S. Li, Y. Wang, T. Tran, A. Perkins, Vibrational spectroscopic studies of (3-mercaptopropyl)trimethoxylsilane sol–gel and its coating. Spectrochim. Acta Part A 61 (2005) 3032–3037. doi:10.1016/j.saa.2004.11.031.

[32] M. Zouari, L. Bois, V. Dugas, S. Hbaieb, Y. Chevalier, R. Kalfat, C. Demesmay, Monolith passive adsorbers prepared with hydrophobic porous silica rods coated with hydrogel. Anal. Lett. 51 (2018) 935–954. doi:10.1080/00032719.2017.1365368.

[33] L. Boksányi, O. Liardon, E.sz. Kováts, Chemically modified silicon dioxide surfaces.Reaction of *n*-alkyldimethylsilanols and *n*-oxaalkyldimethylsilanols with the hydrated surface of silicon dioxide–The question of the limiting surface concentration. Adv. Colloid Interface Sci. 6 (1976) 95–137. doi:10.1016/S0927-7757(00)00556-2.

[34] T. Ji, C. Ma, L. Brisbin, L. Mu, C.G. Robertson, Y. Dong, J. Zhu, Organosilane grafted silica: Quantitative correlation of microscopic surface characters and macroscopic surface properties. Appl. Surf. Sci. 399 (2017) 565–572. doi:10.1016/j.apsusc.2016.11.241.

[35] C. Sulitzky, B. Rückert, A.J. Hall, F. Lanza, K. Unger, B. Sellergren, Grafting of molecularly imprinted polymer films on silica supports containing surface-bound free radical initiators. Macromolecules 35 (2002) 79–91. doi:10.1021/ma011303w.

[36] D. Oliveira, C.P. Gomes, R.C.S. Dias, M.R.P.F.N. Costa, Molecular imprinting of 5-fluorouracil in particles with surface RAFT grafted functional brushes. React. Funct. Polym. 107 (2016) 35–45. doi:10.1016/j.reactfunctpolym.2016.08.007.

[37] C.M. Starks, Free Radical Telomerization. Academic Press, New York (1974).

[38] R.A. Lorenzo, A.M. Carro, C. Alvarez-Lorenzo, A. Concheiro, To remove or not to remove? The challenge of extracting the template to make the cavities available in molecularly imprinted polymers (MIPs). Int. J. Mol. Sci. 12 (2011) 4327–4347. doi:10.3390/ijms12074327.

[39] Y. Fukuhara, Y. Ohzuno, T. Takei, M. Yoshida, Effect of alkyl chain length on adsorption and release of hydrophobic drug to/from hydrophobically-modified gelatin hydrogel. MATEC Web Conf. 333 (2021) 11008. doi:10.1051/matecconf/202133311008.

[40] S.S. Rogers, L. Mandelkern, Glass formation in polymers. I. The glass transitions of the poly(*n*-alkyl methacrylates). J. Phys. Chem. 61 (1957) 985–990. doi:10.1021/j150553a033.

[41] G. Zhao, J. Liu, M. Liu, X. Han, Y. Peng, X. Tian, J. Liu, S. Zhang, Synthesis of molecularly imprinted polymer via emulsion polymerization for application in solanesol separation. Appl. Sci. 10 (2020) 2868. doi:10.3390/APP10082868.

[42] A.L. Hillberg, K.R. Brain, C.J. Allender, Design and evaluation of thin and flexible theophylline imprinted polymer membrane materials. J. Mol. Recognit. 22 (2009) 223–231. doi:10.1002/jmr.935.

[43] J.P. Fan, L. Li, Z.Y. Tian, C.F. Xie, F. Songtian, X.H. Zhang, J.H. Zhu, A novel free-standing flexible molecularly imprinted membrane for selective separation of synephrine in methanol-water media. J. Membrane Sci. 467 (2014) 13–22. doi:10.1016/j.memsci.2014.05.018.

[44] G. Scatchard, The attractions of proteins for small molecules and ions. Ann. New York Acad. Sci. 51 (1949) 660–672. doi:10.1111/j.1749-6632.1949.tb27297.x.

[45] I. Langmuir, The adsorption of gases on plane surfaces of glass, mica and platinum. J. Am. Chem. Soc. 40 (1918) 1361–1403. doi:10.1021/ja02242a004.

[46] S. Ross, J.P. Olivier, On Physical Adsorption, Wiley, New York (1964) p. 17.

[47] D.M. Ruthven, Principles of Adsorption and Adsorption Processes. Wiley, New York (1984) p. 69.

[48] M. Volmer, Thermodynamische Folgerungen ans der Zustandsgleichnng für adsorbierte Stoffe. Z. phys. Chem. 115 (1925) 253–260. doi:10.1515/zpch-1925-11519.

[49] H. Kim, K. Kaczmarski, G. Guiochon, Thermodynamic analysis of the heterogenous binding sites of molecularly imprinted polymers. J. Chromatogr. A 1101 (2006) 136–152. doi:10.1016/j.chroma.2005.09.092.

[50] F. Zhao, E. Repo, D. Yin, M.E. Sillanpää, Adsorption of Cd(II) and Pb(II) by a novel EGTA-modified chitosan material: Kinetics and isotherms. J. Colloid Interface Sci. 409 (2013) 174–182. doi:10.1016/j.jcis.2013.07.062.

[51] P. Shao, D. Liang, L. Yang, H. Shi, Z. Xiong, L. Ding, X. Yin, K. Zhang, X. Luo, Evaluating the adsorptivity of organo-functionalized silica nanoparticles towards heavy metals: Quantitative comparison and mechanistic insight. J. Hazard. Mater. 387 (2020) 121676. doi:10.1016/j.jhazmat.2019.121676.

[52] J. Luo, Y. Gao, K. Tan, W. Wei, X. Liu, Preparation of a magnetic molecularly imprinted graphene composite highly adsorbent for 4-nitrophenol in aqueous medium. ACS Sustain. Chem. Eng. 4 (2016) 3316–3326. doi:10.1021/acssuschemeng.6b00367.

[53] L.D. Marestoni, A. Wong, G.T. Feliciano, M.R.R. Marchi, C.R.T. Tarley, M.D.P.T. Sotomayor, Optimization and application of imprinted poly(AA-EGDMA) for solid phase extraction of ciprofloxacin in artificial urine. Curr. Drug Ther. 9 (2014) 270–276. doi:10.2174/1574885510999150505160637#sthash.I3TiJWc7.dpuf.

[54] Y.C. Wong, Y.S. Szeto, W.H. Cheung, G. McKay, Pseudo-first-order kinetic studies of the sorption of acid dyes onto chitosan. J. Appl. Polym. Sci. 92 (2004) 1633–1645. doi:10.1002/app.13714.

[55] Y.S. Ho, G. McKay, Pseudo-second order model for sorption processes. Process Biochem. 34 (1999) 451–465. doi:10.1016/S0032-9592(98)00112-5.

[56] H. Yuh-Shan, Citation review of Lagergren kinetic rate equation on adsorption reactions. Scientometrics 59 (2004) 171–177. doi:10.1023/b:scie.0000013305.99473.cf.

[57] K.V. Kumar, Pseudo-second order models for the adsorption of safranin onto activated carbon: Comparison of linear and non-linear regression methods. J. Hazard. Mater. 142 (2007) 564–567. doi:10.1016/j.jhazmat.2006.08.018.

[58] Y.S. Ho, Review of second-order models for adsorption systems. J. Hazard. Mater. 136 (2006) 681–689. doi:10.1016/j.jhazmat.2005.12.043.

[59] Y. Wu, Y. Ma, J. Pan, R. Gu, J. Luo, Porous and magnetic molecularly imprinted polymers via Pickering high internal phase emulsions polymerization for selective adsorption of λ-cyhalothrin. Front. Chem. 5 (2017) 18.doi:10.3389/fchem.2017.00018.

[60] S.R. Shafqat, S.A. Bhawani, S. Bakhtiar, M.N.M. Ibrahim, Synthesis of molecularly imprinted polymer for removal of Congo red. BMC Chem. 14 (2020) 27. doi:10.1186/s13065-020-00680-8.

SUPPLEMENTARY INFORMATION

DESIGN OF MOLECULARLY IMPRINTED POLYMER MATERIALS RELYING ON HYDROPHOBIC INTERACTIONS

Najeh Jaoued[1], Chaima Nasraoui[2,3], Yves Chevalier[3,]*, Souhaira Hbaieb[2,]*

1- *Unité Spécialisée de développement des techniques analytiques, Institut National de Recherche et d'Analyse Physico-chimique, Biotechpole Sidi-Thabet, 2020 Ariana, Tunisia.*
2- *Laboratoire de Recherche: Caractérisations, Applications et Modélisation de Matériaux, Université de Tunis El Manar, Faculté des Sciences de Tunis, Campus universitaire El Manar, Tunisia.*
3- *Laboratoire d'Automatique, de Génie des Procédés et de Génie Pharmaceutique, Université de Lyon 1, UMR 5007 CNRS, 43 bd 11 Novembre, 69622 Villeurbanne, France.*

* Corresponding authors:
Souhaira Hbaieb: souhaira.hbaieb@fst.utm.tn; tel: +216 71 88 34 24; fax: +216 71 80 25 36
Yves Chevalier: yves.chevalier@univ-lyon1.fr; tel: +33 472 43 18 77

S1. Grafting of 3-MPTMS on the silica surface

Grafting 3-mercaptopropyltrimethoxysilane silane (3-MPTMS) to the surface of silica was achieved by a direct reaction in anhydrous aprotic medium (toluene). It involves the reaction of surface silanols of silica with the methoxy groups of 3-MPTMS according to Scheme S1. Such process allows binding a dense monolayer at the surface of silica.

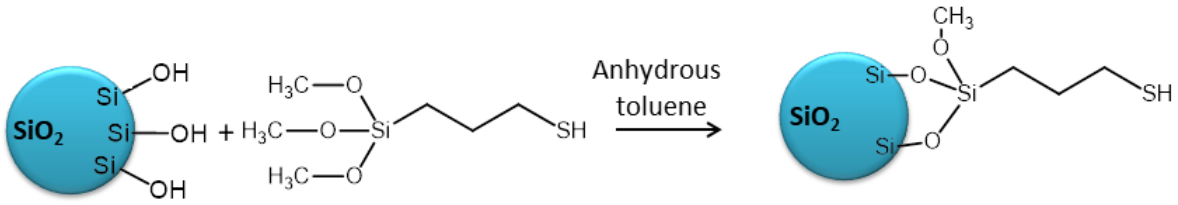

Scheme S1. Synthesis scheme of MPTMS-modified SiO_2 particles.

The IR spectra of pristine and grafted silica (Figure S1) show common bands pertaining to silica and additional bands for the grafted material. A sharp and strong absorption band at 1010–1190 cm^{-1} and a weaker band at 800–900 cm^{-1} ascribed to the Si–O–Si stretching of silica for both samples. As expected, there was no significant change of these bands upon surface modification. The band appearing at 3000–3600 cm^{-1} corresponds to O–H stretching vibrations of the surface silanol groups. It is broad for unmodified silica because the surface density of Si–OH is high, allowing extensive hydrogen bonds between them. Indeed, hydrogen-bonded O–H

groups give rise to a broad IR absorption band centered at 3300 cm^{-1}. Isolated O–H groups are characterized by a sharp band at 3600 cm^{-1}. Grafting organosilane considerably sharpened the O–H band and shifted it to higher wavenumber (Figure S1 inset). This indicated that a significant part of the Si–OH groups turned isolated because their neighbors have been grafted. There remained hydrogen-bonded O–H groups however, as revealed by a residual broad absorption band extending down to 3400 cm^{-1}. As summary, IR spectroscopy revealed that the density of Si–OH has been considerably decreased. Conversion of Si–OH did not reach completion however. Indeed, the surface density of silanol groups of bare silica (~ 6 $\mu mol \cdot m^{-2}$) [1] is much larger than the maximum grafting density of a dense close-packed monolayer of organosilane (2–4 $\mu mol \cdot m^{-2}$) [2]. Therefore, there was quite a significant amount of residual Si–OH groups buried beneath the layer of organosilane. The IR spectrum of modified silica showed two supplementary bands, a double peak at 2928–2858 cm^{-1} related to CH_2 stretching vibrations, which demonstrates that 3-MPTMS has been extensively grafted on the silica surface, and a weak band at 2575 cm^{-1} related to –SH group [3].

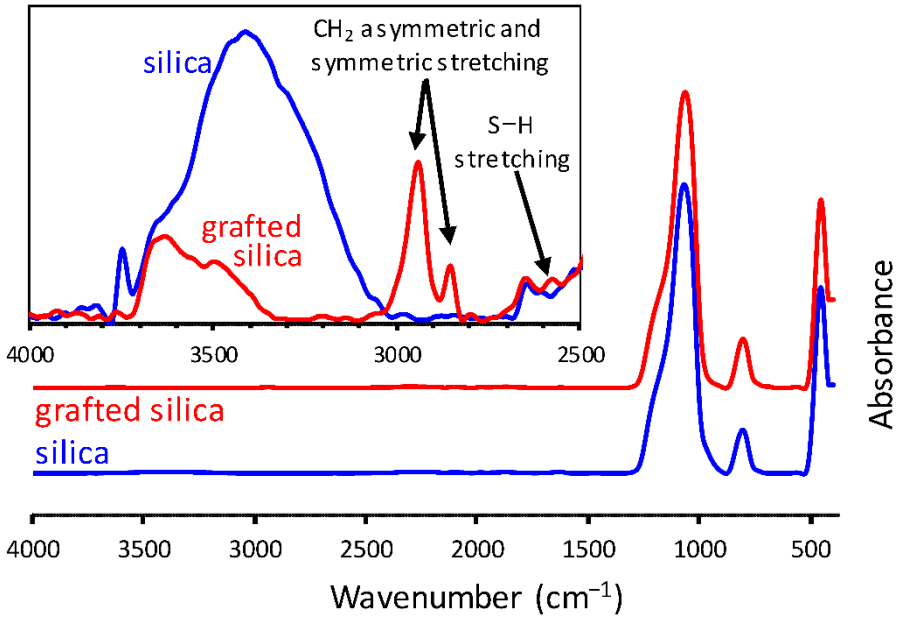

Figure S1. IR spectra of dehydrated and MPTMS-modified SiO_2 particles. The 2500–4000 cm^{-1} region is expanded in the inset.

The ^{29}Si and ^{13}C CP-MAS NMR spectra of dehydrated and MPTMS-modified SiO_2 particles are shown in Figure S2 and Figure S3, respectively. The ^{29}Si CP-MAS spectrum of unmodified silica (Fig S2A) shows lines centered at −99, −102 and −110 ppm due to the different Si species. The peak at −99 ppm is attributed to Si atoms having two attached hydroxyl groups, $(Si\text{-}O)_2Si(OH)_2$ referred to as Q_2. Two peaks arising from the silicon environments of the hydroxyl group (single silanol), $(SiO)_3Si\text{-}OH$ (Q_3) and $Si(OSi)_4$ (Q_4) units, were observed at −102 and

−110 ppm respectively [4]. Supplementary peaks were observed at −64, −58 and −51 ppm in the spectrum of modified silica (Figure S2B), indicating the presence of T_3, T_2 and T_1 units respectively, coming from Si atoms of the functionalizing agent (3-MPTMS). The intensity of the Q_2 and Q_3 peaks has also decreased upon grafting, confirming that the surface silanol groups were the sites for grafting mercaptopropylsilyl groups [5]. The ^{13}C CP-MAS NMR spectrum of the modified silica sample (Figure S3) clearly shows the peaks of carbons belonging to 3-MPTMS moieties. The signal related to the methylene group of 3-MPTMS directly bonded to the silicon atom (Si-$\underline{CH_2}$) is observed at 14 ppm and another peak at 29 ppm is assigned to the methylene carbon atoms in α and β-position of SH group ($\underline{C}H_2$-$\underline{C}H_2$-SH). The signal at 50 ppm is assigned to residual SiO$\underline{CH_3}$ resulting from the incomplete condensation reaction of methoxy groups.

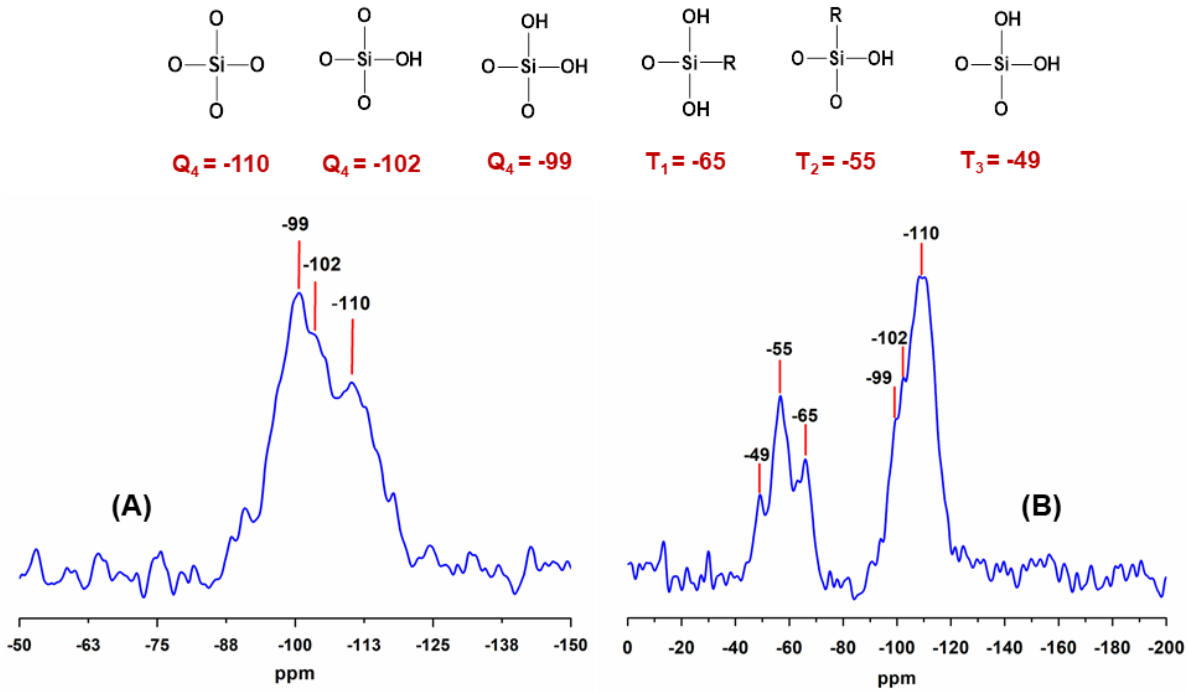

Figure S2. ^{29}Si CP-MAS NMR spectra of dehydrated (A) and MPTMS-modified (B) silica.

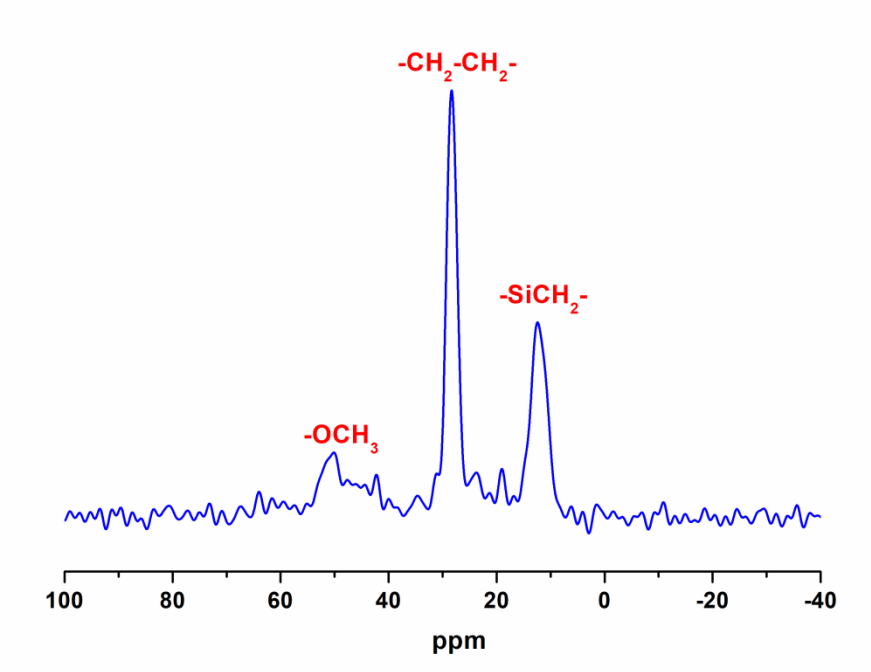

Figure S3. ^{13}C CP-MAS NMR spectrum of SiO_2@MPTMS.

The grafting density was calculated from elemental analyses of sulfur (%S) taking the specific area A_{sp} = 200 $m^2 \cdot g^{-1}$ as:

$$\textit{Surface density}\ (\text{mol}\cdot\text{m}^{-2}) = \frac{\%S}{100 \times 32.065 \times A_{sp}} \qquad \text{(S-1)}$$

A surface density of 5.4 µmol·m^{-2} was inferred from the %S of 3.48 %.

It was also calculated from the mass loss measured by thermogravimetric analysis (TGA). A single mass loss was observed between 300 and 450 °C (Figure S4). The onset of thermal degradation was at ~ 300 °C. The corresponding mass loss was estimated as the distance between tangents to the high and low temperature branches. Given that thermal degradation took place at the Si–(organic matter) chemical bond, leaving a Si–H residue, the grafting density was calculated taking the molar mass of the lost organic moiety $-(CH_2)_3-SH$ of 75 g·mol^{-1} as:

$$\textit{Surface density}\ (\text{mol}\cdot\text{m}^{-2}) = \frac{\%\text{mass loss}}{100 \times 75 \times A_{sp}} \qquad \text{(S-2)}$$

A surface density of 4.8 µmol·m^{-2} was inferred from the mass loss of 7.17 %.

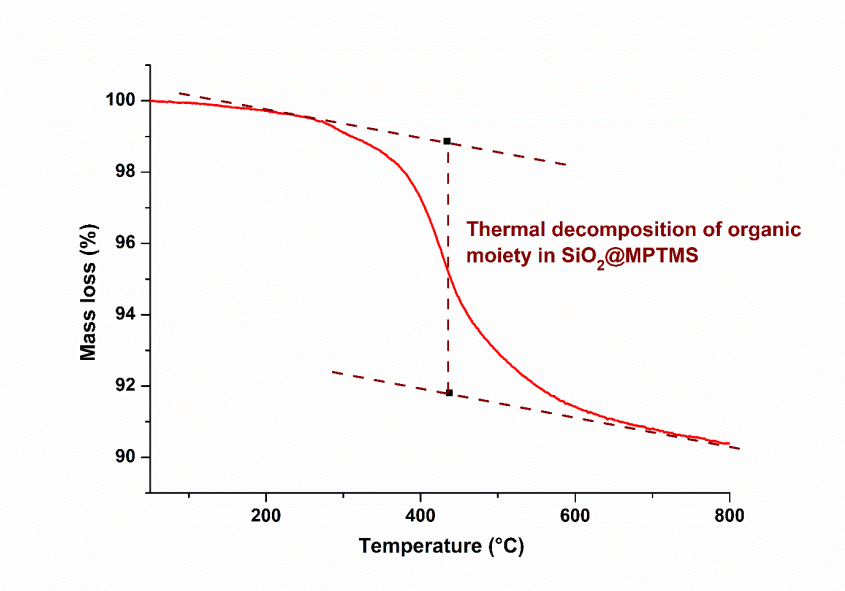

Figure S4. TGA of SiO_2@MPTMS.

S2. Synthesis of the MIP and NIP materials

The recipes for the synthesis of the MIP and NIP by polymerization of the different functional monomers and the cross-linking agent are given in Table S1.

Table S1. Polymerization recipe conditions for the preparation of materials. The selected recipe is marked in green color.

MIP and NIP materials	Silica ($g \cdot L^{-1}$)	Monomer ($mmol \cdot L^{-1}$)	Cross-linking agent ($mmol \cdot L^{-1}$)	[Mit] for MIP ($mmol \cdot L^{-1}$)
SiO_2@$MMAC_2$	20	50	50	16
SiO_2@$MMAC_6$	20	50	50	16
SiO_2@$BMAC_2$	20	50	50	16
SiO_2@$BMAC_6$	20	50	50	16
SiO_2@$LMAC_2$-1	20	50	50	16
SiO_2@$LMAC_6$-1	20	50	50	16
SiO_2@$LMAC_2$-2	20	160	100	16
SiO_2@$LMAC_6$-2	20	160	100	16
SiO_2@$LMAC_2$-3	20	160	160	16
SiO_2@$LMAC_6$-3	20	160	160	16
SiO_2@$LMAC_2$-4	20	160	320	16
SiO_2@$LMAC_6$-4	20	160	320	16

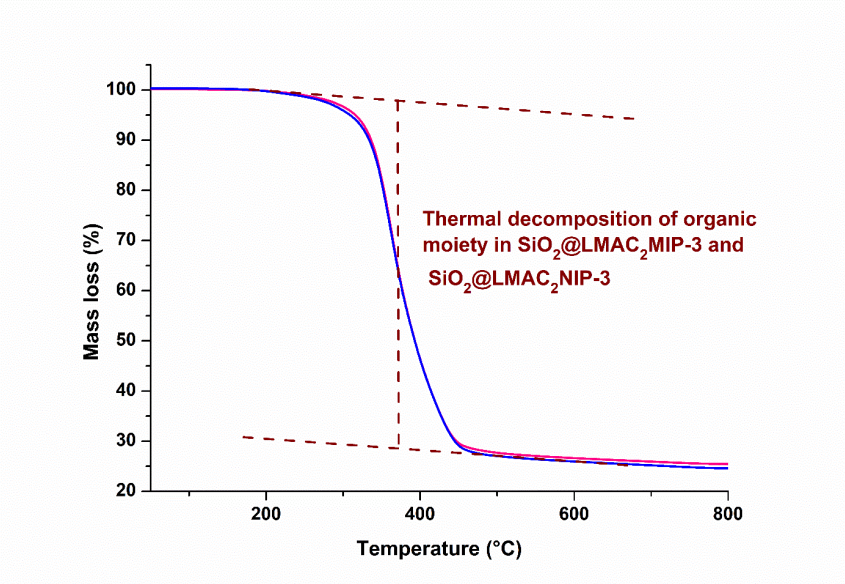

Figure S5. TGA of SiO_2@$LMAC_2$MIP-3 and SiO_2@$LMAC_2$NIP-3.

Table S2. Elemental and TGA analyses of MIP and NIP materials, and their adsorption properties: equilibrium adsorbed amount (*Q*e) and imprinting factor (*IF*) at 25 °C in 10 mL of a mixed of water/methanol (50/50 v/v) solution of Mit 7.5 10^{-5} mol·L^{-1}. The selected material is marked in green color.

MIP and NIP materials	%C	Mass loss (%)	*Q*e (mg·g^{-1})	*IF*
SiO_2@$MMAC_2$MIP	27.8	41.9	18.4	1.30
SiO_2@$MMAC_2$NIP	28.0	42.2	14.1	
SiO_2@$MMAC_6$MIP	31.5	46.3	18.5	1.28
SiO_2@$MMAC_6$NIP	31.7	46.7	14.5	
SiO_2@$BMAC_2$MIP	30.5	45.6	18.5	1.58
SiO_2@$BMAC_2$NIP	30.6	45.9	11.7	
SiO_2@$BMAC_6$MIP	32.9	47.3	19.6	1.54
SiO_2@$BMAC_6$NIP	33.0	48.1	12.7	
SiO_2@$LMAC_2$MIP-1	35.5	52.3	20.4	1.81
SiO_2@$LMAC_2$NIP-1	35.6	52.7	11.3	
SiO_2@$LMAC_6$MIP-1	36.9	55.1	20.6	1.77
SiO_2@$LMAC_6$NIP-1	37.1	55.8	11.6	
SiO_2@$LMAC_2$MIP-2	40.9	61.7	19.9	1.71
SiO_2@$LMAC_2$NIP-2	41.0	62.2	11.8	
SiO_2@$LMAC_6$MIP-2	43.6	68.5	19.9	1.56
SiO_2@$LMAC_6$NIP-2	43.8	68.8	12.8	
SiO_2@$LMAC_2$MIP-3	47.6	70.7	21.0	2.40
SiO_2@$LMAC_2$NIP-3	47.9	71.9	8.7	
SiO_2@$LMAC_6$MIP-3	53.6	73.3	21.4	1.92
SiO_2@$LMAC_6$NIP-3	53.9	74.2	11.1	
SiO_2@$LMAC_2$MIP-4	55.6	82.7	22.0	2.22
SiO_2@$LMAC_2$NIP-4	55.7	83.0	9.9	
SiO_2@$LMAC_6$MIP-4	56.7	86.2	22.1	2.10
SiO_2@$LMAC_6$NIP-4	56.9	86.8	10.5	

[1] L.T. Zhuravlev, The surface chemistry of amorphous silica. Zhuravlev model. Colloids Surf. A 173 (2000) 1–38. doi:10.1016/S0927-7757(00)00556-2.
[2] L. Boksányi, O. Liardon, E.sz. Kováts, Chemically modified silicon dioxide surfaces. Reaction of *n*-alkyldimethylsilanols and *n*-oxaalkyldimethylsilanols with the hydrated surface of silicon dioxide–The question of the limiting surface concentration. Adv. Colloid Interface Sci. 6 (1976) 95–137. doi:10.1016/S0927-7757(00)00556-2.
[3] G. Socrates, Infrared and Raman Characteristic Group Frequencies. 3rd ed., Wiley, Chichester (2001) p. 209.
[4] M. Zouari, L. Bois, V. Dugas, S. Hbaieb, Y. Chevalier, R. Kalfat, C. Demesmay, Monolith passive adsorbers prepared with hydrophobic porous silica rods coated with hydrogel. Anal. Lett. 51 (2018) 935–954. doi:10.1080/00032719.2017.1365368.
[5] F. Arfaoui, N. Jaoued-Grayaa, A. Riani Khlifi, R. Kalfat, Synthesis and characterization of molecularly imprinted silica for efficient adsorption of melamine. J. Tun. Chem. Soc. 19 (2017) 227–236. http://www.sctunisie.org/pdf/JSCT_v19-31.pdf.